


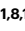









Distinct baseline immune characteristics associated with responses to conjugated and unconjugated pneumococcal polysaccharide vaccines in older adults

Received: 21 April 2023

Accepted: 21 November 2023

Published online: 5 January 2024

 Check for updates

Sathyabaarathi Ravichandran ^{1,11}, Fernando Erra-Diaz ^{1,8,11},
Onur E. Karakaslar ^{1,9,11}, Radu Marches¹, Lisa Kenyon-Pesce², Robert Rossi ¹,
Damien Chaussabel ¹, Djamel Nehar-Belaid ¹, David C. LaFon³,
Virginia Pascual ⁴, Karolina Palucka¹, Silke Paust ^{1,5}, Moon H. Nahm³,
George A. Kuchel ², Jacques Banchereau^{1,10} & Duygu Ucar ^{1,6,7} 

Pneumococcal infections cause serious illness and death among older adults. The capsular polysaccharide vaccine PPSV23 and conjugated alternative PCV13 can prevent these infections; yet, underlying immunological responses and baseline predictors remain unknown. We vaccinated 39 older adults (>60 years) with PPSV23 or PCV13 and observed comparable antibody responses (day 28) and plasmablast transcriptional responses (day 10); however, the baseline predictors were distinct. Analyses of baseline flow cytometry and bulk and single-cell RNA-sequencing data revealed a baseline phenotype specifically associated with weaker PCV13 responses, which was characterized by increased expression of cytotoxicity-associated genes, increased frequencies of CD16⁺ natural killer cells and interleukin-17-producing helper T cells and a decreased frequency of type 1 helper T cells. Men displayed this phenotype more robustly and mounted weaker PCV13 responses than women. Baseline expression levels of a distinct gene set predicted PPSV23 responses. This pneumococcal precision vaccinology study in older adults uncovered distinct baseline predictors that might transform vaccination strategies and initiate novel interventions.

Streptococcus pneumoniae (pneumococcus) infections lead to life-threatening diseases and are responsible for thousands of hospitalizations and deaths annually in the United States¹. Infants and older adults have the highest rates of invasive pneumococcal disease, with an ~10% mortality rate particularly affecting older adults according to reports from the Centers for Disease Control and Prevention reports. Two types of pneumococcal vaccines were approved by the Food and Drug Administration (FDA) for use in this population: the capsular polysaccharide vaccine Pneumovax[®] (PPSV23) and protein-polysaccharide

conjugate vaccines (for example, Prevnar[®] (PCV13)). PPSV23 contains capsular polysaccharide antigens for 23 serotypes that elicit antibody responses in the absence of CD4⁺ T cell collaboration². Responses to unconjugated polysaccharides are predominantly mediated by the activation of marginal zone (MZ) B cells, which possess hypermutated immunoglobulin genes and express high levels of complement receptor 2 (CD21)^{3,4}. MZ B cells are not fully mature in newborns and children, resulting in limited success of unconjugated polysaccharide vaccines^{3,5,6}. Furthermore, older individuals show a marked decrease

A full list of affiliations appears at the end of the paper. ✉ e-mail: duygu.ucar@jax.org

in frequencies of total memory and MZ B cells, which might contribute to the age-related decline of responses⁷. After activation, MZ B cells terminally differentiate into IgM-, IgG- and IgA-secreting plasma cells⁸. Although MZ B cell activation and IgM production are considered to be T cell independent, IgG and IgA class switching might rely on the presence of non-cognate T cells that secrete IL-21 and/or trigger the CD40/CD40L signaling axis⁹. Conjugated vaccines have been developed (for example, PCV13) to enhance immunogenicity. PCV13 is composed of polysaccharides for the most prevalent 13 serotypes conjugated to a nontoxic variant of diphtheria toxin CRM197. PCV13 induces T cell-dependent activation and expansion of B2 follicular cells, promoting the generation of memory B cells and differentiation of long-lived plasma cells^{9–11}.

Conjugated pneumococcal vaccines are effective among children and young adults¹ and in preventing invasive disease among older adults¹², yet their efficacy declines with age^{13–15}. PCV13 is 90% effective in infants and children, which decreases to 72.8% among older adults. Similarly, the efficacy of PPSV23 is 54% for adults¹⁶. In 2021, other conjugated vaccines were approved, including PCV15 and PCV20, to extend the range of serotypes covered and to simplify pneumococcal immunizations¹⁷. In the United States, the current recommendation for older adults is to receive either PCV20 or PCV15 followed by PPSV23 1 year later.

Peripheral blood leukocyte gene expression studies revealed transcriptional differences in responses to PPSV23 and influenza vaccines among healthy adults^{18,19}. However, these studies did not include conjugated pneumococcal vaccines and excluded older adults partially due to the complexity of evaluating their responses. To address these gaps, we recruited 39 healthy pneumococcal vaccine-naïve adults ≥60 years old who received PCV13 or PPSV23. We collected blood from this cohort longitudinally and studied their baseline immune phenotypes and immune responses following vaccination by using multiple assays. Our systems vaccinology approach uncovered distinct baseline gene expression modules associated with PCV13 and PPSV23 responses, which can pave the way toward more precise administration of these vaccines.

Results

Serological responses of older adults to PCV13 and PPSV23

During the 2017–2018 seasons, 39 older adults (≥60 years of age with no history of pneumonia disease or vaccination) were recruited and randomized to receive either a dose of PCV13 (ten men and nine women) or PPSV23 (ten men and ten women). Vaccines were administered from May to early fall to avoid overlap with the influenza vaccine season. Donors in each arm of the study and the men and women in each arm were comparable in terms of age, body mass index (BMI), cytomegalovirus (CMV) seropositivity and frailty index (Fig. 1a). Donors were not on any confounding treatments, but some were on medications for common chronic diseases (Supplementary Table 1a,b).

Blood samples were collected 7 d before vaccination (baseline) and at 1, 10, 28 and 60 d after vaccination. Previously, we showed that transcriptional innate responses to PPSV23 peaked at day 1, whereas adaptive responses peaked at day 7 and remained high until day 14 in adults¹⁹. Hence, days 1 and 10 were chosen to capture the innate and adaptive responses while also ensuring participant safety and adherence to the institutional review board recommendations regarding the maximum volume of blood one can collect from older adults (550 ml over an 8-week period or 69 ml per week). We generated longitudinal flow cytometry and RNA-sequencing (RNA-seq) data to study immune responses to these two vaccines (Fig. 1a). Pneumococcal vaccine responses can be assessed by measuring antibody levels using enzyme-linked immunosorbent assays (ELISAs) or antibody function using opsonophagocytic activity (OPA). OPA measures the ability of antibodies to effectively opsonize bacteria and is ideal for quantifying responses because it mimics the in vivo mechanisms of antibody protection²⁰ and is hence considered state of the art for FDA approvals²¹. Unlike children, many older adults already possess high ELISA antibody levels before vaccination, making functional OPA assays more attractive in this population²⁰. Therefore, we used OPA to quantify antibody responses from serum (at baseline and 28 d after vaccination). Because OPA assays require a substantial volume of serum, we prioritized the 13 most prevalent serotypes: the 12 shared serotypes and serotype 6A from PCV13 (Supplementary Table 2)²². Quantifying the common serotypes enabled a side-by-side comparison of these two vaccines.

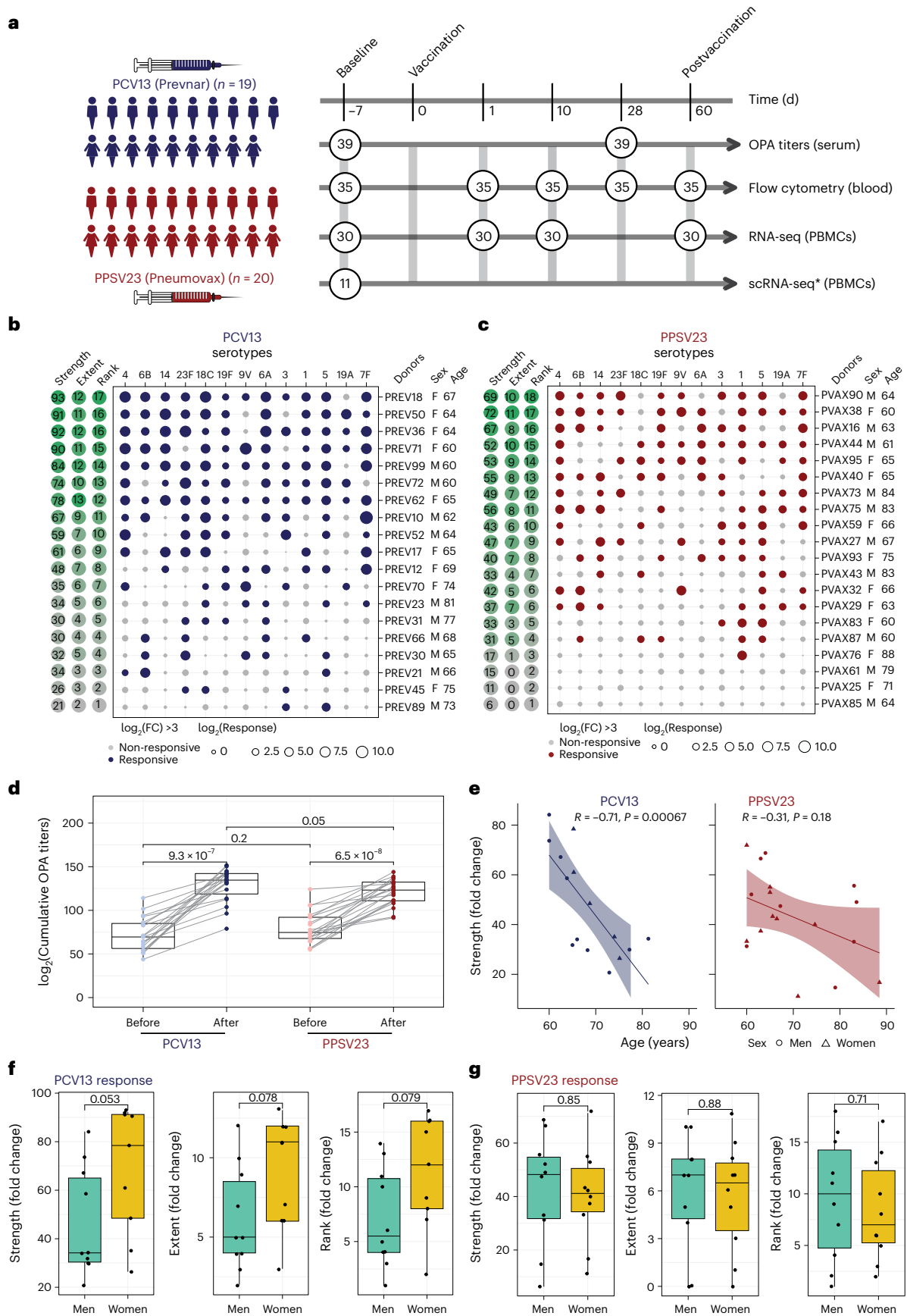
We developed three multivariate measures to quantify vaccine responses: (1) strength of the response (the sum of fold change values between baseline and day 28 for all serotypes), (2) extent (the number of serotypes (of 13) to which the donor elicits significant (that is, an OPA titer of ≥8) responses) and (3) rank (the rank of an individual's vaccine responsiveness in the cohort based on aggregate responses for all serotypes, where higher ranks represent stronger responses; Fig. 1b,c, Extended Data Fig. 1a,b and Supplementary Table 2d,h). To assess whether quantifying PPSV23 responses using 13 serotypes fully captures responsiveness to this vaccine, we reanalyzed OPA titers for all 23 serotypes from another study¹¹, which revealed a strong and significant correlation between ranking using 13 serotypes and ranking using all serotypes ($R = 0.91$, $P = 0.013$; Extended Data Fig. 1g). Strength and extent of responsiveness were highly correlated with the rank, while capturing different aspects of vaccine responses (Extended Data Fig. 1c). BMI, frailty index and number of concomitant medications were not associated with responsiveness to either vaccine (Extended Data Fig. 1d and Supplementary Table 1a,b).

After vaccination, OPA titer levels significantly increased for both vaccines cumulatively (Fig. 1d) and for each serotype (Extended Data Fig. 1e). Stronger PCV13 responses were detected for serotype 4 and the PCV13-specific serotype 6A (Extended Data Fig. 1e). Although PPSV23

Fig. 1 | Functional antibody response to PCV13 and PPSV23 in older adults.

a, Schematic representation of the study design. Nine women and ten men received the PCV13 vaccine, and ten women and ten men received PPSV23. OPA titers for the 13 serotypes were assessed from serum samples obtained 7 d before vaccination (baseline) and 28 d after vaccination for both vaccines. Anticoagulated blood samples were used for flow cytometric analysis of whole-blood cell populations. PBMCs were isolated for bulk RNA-seq. Prevacination PBMCs from four women and seven men who received PCV13 were isolated for scRNA-seq. The numbers in circles represent the total numbers of biologically independent samples processed for the indicated assays at the indicated times. Figure created with [BioRender.com](https://www.biorender.com). The star indicates scRNA-seq data generated exclusively for the PCV13 baseline samples. **b**, Bubble plot of fold change (FC) in antibody titers for individual serotypes in response to PCV13 ($n = 19$); M, male; F, female. **c**, Bubble plot of fold change in antibody titers for individual serotypes in response to PPSV23 ($n = 20$). Dot size represents the fold change value, and color indicates a significant response ($\log_2(\text{fold change}) > 3$), with blue for PCV13 and red for PPSV23. Donors are ordered from top

to bottom according to the vaccine response rank. On the left, the strength ($\log_2(\text{sum fold change})$), extent of response (number of serotypes out of 13 to which an individual mounted a significant response) and rank are presented. **d**, Prevacination and postvaccination cumulative OPA titers (expressed as sum \log_2 in response to PCV13 ($n = 19$) and PPSV23 ($n = 20$)). **e**, Correlation analysis between the cumulative fold change (sum $\log_2(\text{fold change})$) and age (in years). **f,g**, Sex-specific differences in strength, extent and rank in donors who received PCV13 ($n = 19$; **f**) and PPSV23 ($n = 20$; **g**). A Wilcoxon matched-pairs signed-rank test (two sided) was used in **d** to compare titers before and after vaccination with PCV13 or PPSV23. Box plots display the median and interquartile range (IQR; 25–75%), with whiskers representing the upper and lower quartiles $\pm 1.5 \times \text{IQR}$. A Wilcoxon rank-sum test (two sided) was used to compare strength, extent and rank between men and women vaccinated with PCV13 and PPSV23. The Pearson correlation metric was used to perform correlation analyses between strength and age (**e**), and P values were computed using two-sided t -tests; n represents the number of biological replicates.



does not contain serotype 6A, it induced increased 6A responses potentially due to cross-reactivity with serotype 6B. Baseline OPA titers were comparable between the two cohorts ($P = 0.2$); however, individuals vaccinated with PCV13 had stronger responses (Fig. 1d; $P = 0.05$) even after excluding serotype 6A ($P = 0.089$; Extended Data Fig. 1f). Level of responsiveness varied from one individual to another. In the group treated with PCV13, top responder PREV18 (female, 67 years old) responded significantly to all serotypes except for 19A, whereas the bottom responder PREV89 (male, 73 years old) elicited significant responses to only two serotypes (Fig. 1b). In PPSV23, top responder PVAX90 (male, 64 years old) responded to ten serotypes, whereas the bottom responder PVAX25 (female, 71 years old) did not respond significantly to any of the tested serotypes (Fig. 1c). Our ranking strategy captured this heterogeneity at the donor level. There was a significant inverse correlation between baseline OPA titer levels and fold change in titers (Extended Data Fig. 2a–c), in alignment with previous studies²³. There was a significant negative correlation between cumulative OPA titers at baseline and vaccine responsiveness rank (Extended Data Fig. 2d). Given this association, we calculated the maximum residual after baseline adjustment (maxRBA) values (Extended Data Fig. 1a,b), which correct for baseline titer levels by modeling fold increase in titer levels as an exponential function of the baseline titer levels. maxRBA and rank correlated significantly for both vaccines (Extended Data Fig. 1c).

Donor age was negatively associated with both strength (Fig. 1e; $R = -0.71$ and $P = 0.00067$ for PCV13, $R = -0.31$ and $P = 0.18$ for PPSV23) and rank (Extended Data Fig. 2d). Although male and female donors were comparable in terms of age, frailty and BMI (Supplementary Table 1b), women mounted stronger responses to the PCV13 vaccine ($P = 0.053$ for strength, $P = 0.079$ for rank; Fig. 1f), which was not observed for PPSV23 (Fig. 1g). Four of five top responders were women and four of five bottom responders were men in the group treated with PCV13. Overall, these data showed that both pneumococcal vaccines induced strong antibody responses; yet, at the individual level, the degree of responsiveness was variable. For PCV13, donor age significantly contributed to this variation, and there was a trend for stronger responsiveness for women. Interestingly, neither age nor sex was significantly associated with PPSV23 responsiveness.

PCV13 and PPSV23 induce similar transcriptional responses

We generated longitudinal bulk RNA-seq data at baseline and days 1, 10 and 60 from peripheral blood mononuclear cells (PBMCs) from 31 donors (15 PCV13 and 16 PPSV23), including strong responders (SRs) and weak responders (WRs) for each vaccine while also balancing female and male samples. Samples from 30 donors that passed quality control were used in differential analyses. Gene expression profiles after vaccination were compared to those at baseline (day -7; Supplementary Table 3). There were no significant transcriptional changes for days 1 or 60. However, at day 10, 50 and 41 genes were differentially expressed compared to baseline (false discovery rate (FDR) < 0.05), respectively, for PCV13 and PPSV23 (Extended Data Fig. 3a). Upregulated genes after vaccination included immunoglobulin heavy chain genes *IGHG2* and *IGHA2* and plasmablast-associated genes *JCHAIN* and *MZB1* (Fig. 2a). The activity of these genes peaked at day 10 and returned to baseline levels by day 60 (Fig. 2b). A cumulative plasmablast activity score using plasma cell-specific genes¹⁹ ($n = 33$ genes) confirmed a significant and comparable increase in the expression of plasmablast-associated genes at day 10 for both vaccines that returned to baseline levels at day 60 (Fig. 2b). *IGHG2*, encoding the IgG2 isotype, was among the most upregulated genes for both vaccines (Fig. 2c). *IGHA2*, encoding the IgA2 isotype, was also upregulated for both vaccines (Fig. 2c and Extended Data Fig. 3b), in alignment with the serology data²⁴.

Pneumococcal vaccines upregulated distinct immunoglobulin genes compared to the influenza vaccine. Reanalysis of prior PBMC RNA-seq data on influenza vaccine responses in younger adults showed upregulated expression of *IGHG1* and *IGHG3* at day 7, whereas

pneumococcal vaccines upregulated the expression of *IGHA2* and *IGHG2* (Fig. 2d and Extended Data Fig. 3c). Transcriptional activation of plasmablast-associated genes significantly correlated with PCV13 responsiveness ($R = 0.57$, $P = 0.034$), mainly driven by *IGHG2* expression (Extended Data Fig. 3d,f), which was not the case for PPSV23 (Extended Data Fig. 3e,f). Together, transcriptional profiling before and after vaccination revealed that both pneumococcal vaccines induced significant and similar plasmablast responses 10 d after vaccination, including increased transcription of genes encoding IgG2 and IgA2 antibody isotypes, contrasting with those (IgG1, IgG3 and IgA1) induced by the influenza vaccine.

Baseline frequencies of T_{H1} and T_{H17} cells are linked to PCV13 responses

We performed a longitudinal flow cytometry analysis of different cell populations in freshly isolated PBMCs at baseline (day -7) and after vaccination at days 1, 10, 28 and 60 to study B cell (naive, memory and plasmablast cells), $CD4^+$ T cell (naive, type 1 helper T (T_{H1}), type 2 helper T (T_{H2}), interleukin-17 (IL-17)-producing helper T (T_{H17}), IL-10-producing helper T (T_{H10}), follicular helper T (T_{FH}), type 1 T_{FH} (T_{FH1}), type 2 T_{FH} (T_{FH2}) and IL-17-producing T_{FH} (T_{FH17}) cells) and dendritic cell (DC) subsets (type 2 classical DCs (cDC2s), type 1 cDCs (cDC1s) and plasmacytoid DCs (pDCs); Supplementary Table 4a and Extended Data Fig. 4a,b). Despite the robust plasmablast transcriptional signature, their absolute numbers were only marginally increased at day 10 for both vaccines (Fig. 3a, top). There were no significant changes in other B cell subsets after vaccination or between the two cohorts (Extended Data Fig. 4b). Among the studied T cell subsets, only $ICOS^+$ T_{FH} cell numbers significantly increased at day 10 for both vaccines (Fig. 3a, bottom, and Extended Data Fig. 4b). There were no significant changes in other T cell or DC subsets after vaccination (Extended Data Fig. 4b). Cell numbers were similar between the two cohorts for all cell types both at baseline and after vaccination (Extended Data Fig. 4b). Therefore, the most significant changes included an increase in plasmablasts and $ICOS^+$ T_{FH} cells at day 10, which was comparable between the two vaccines. However, unlike our previous observations for influenza vaccines²⁵, changes in these cell types did not correlate with vaccine responsiveness (Extended Data Fig. 4c).

To uncover baseline cellular predictors, we performed correlation analyses between the prevaccination absolute cell numbers for B cell, T cell and DC subsets and vaccine responsiveness (rank) for each vaccine. None of the profiled cell types were significantly associated with PPSV23 (Fig. 3b). By contrast, T_{H1} cell frequency ($R = 0.74$, $P = 0.0012$) was positively associated with PCV13 responses, while proinflammatory T_{H17} cell frequency ($R = -0.72$, $P = 0.0015$) was negatively associated with PCV13 responses (Fig. 3b,c; see Extended Data Fig. 5a,b for cell numbers). The ratio of T_{H1} cell frequency to T_{H17} cell frequency was the strongest predictor of PCV13 responses ($R = 0.63$, $P = 0.0089$) but not PPSV23 responses (Fig. 3b and Extended Data Fig. 5c). There was no significant difference in T_{FH} frequency between SRs and WRs, although T_{FH1} cells showed a positive association with PCV13 responsiveness, and T_{FH17} cells showed a negative association with PCV13 responsiveness (Fig. 3b). We observed sex differences in T_{H1} and T_{H17} cell frequencies; women had higher T_{H1} ($P = 0.012$) and lower T_{H17} cell frequencies ($P = 0.028$) than men (Fig. 3d and Extended Data Fig. 5c). Women with higher T_{H1} : T_{H17} cell ratios mounted stronger responses to PCV13 (Extended Data Fig. 5c). These two cell types and their ratios were not significantly associated with age (Fig. 3e). Together, these data established that individuals with higher frequencies of T_{H1} cells and lower frequencies of T_{H17} cells before vaccination mount stronger responses to the conjugated PCV13 vaccine.

Baseline CYTOX level is negatively associated with PCV13 responses

To identify baseline transcriptional signatures associated with vaccine responsiveness, we conducted weighted gene coexpression network

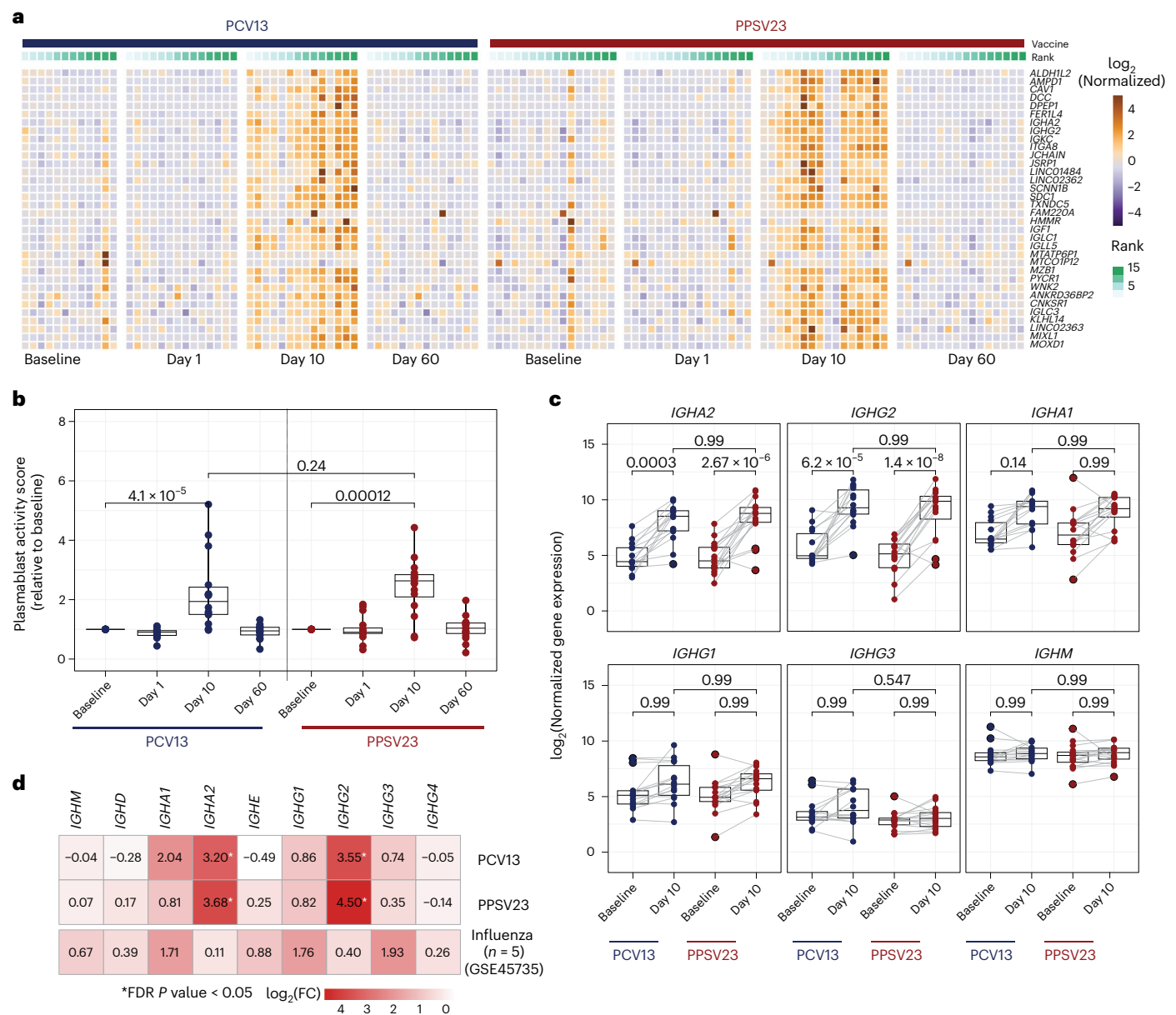


Fig. 2 | Plasmablast response elicited after vaccination at day 10 in PBMCs.

a, Heat map of differentially expressed genes between day 10 and baseline assessed using normalized gene expression values. **b**, Box plot of plasmablast activity scores at baseline and days 1, 10 and 60 in response to PCV13 ($n = 14$) and PPSV23 ($n = 16$), calculated using a published gene set (M4.11) and scaled with reference to baseline. **c**, Box plots showing normalized expression of genes encoding the constant region of the immunoglobulin heavy chain structure in response to PCV13 ($n = 14$) and PPSV23 ($n = 16$). **d**, Heat map showing differential expression of genes encoding the constant region of the immunoglobulin heavy chain structure at day 10 in response

to PCV13 ($n = 14$) and PPSV23 ($n = 16$) and at day 7 in response to Fluzone (GSE45735 (influenza vaccine); $n = 5$). Genes with a >1.5-fold difference and FDR-corrected P value of <0.05 are marked with an asterisk (*). A Wilcoxon rank-sum test (two sided) was used to compare plasma cell activity scores between baseline and days 1, 10 and 60 (**b**). Box plots display the median and IQR (25–75%), with whiskers representing the upper and lower quartiles $\pm 1.5 \times$ IQR. A Wilcoxon matched-pairs signed-rank test (two sided) was used to compare the expression of immunoglobulin genes at baseline and day 10 for PCV13 and PPSV23. FDR-corrected P values are shown in **c**; n represents the number of biological replicates.

analysis (WGCNA) on PBMC RNA-seq data, which yielded 33 gene modules. We associated these modules with vaccine responsiveness, sex, age and $T_H1:T_H17$ cell ratio. Of 33 modules, only 1 (midnight blue, 260 genes) was significantly ($P = 0.02$) and specifically associated with PCV13 responses (Extended Data Fig. 6a and Supplementary Table 5a). Genes in this module were enriched in the ‘natural killer cell mediated cell cytotoxicity’ KEGG pathway ($P = 0.000003639$) and included *NCAMI*, the marker gene for natural killer (NK) cells, and several transcripts (*GNLY*, *PRF1* and *GZMB*) encoding cytotoxic functions²⁶ (Supplementary Table 6a). This cytotoxicity-associated gene module is hereafter referred to as the CYTOX module. Baseline expression levels

of CYTOX genes in PBMCs was negatively associated with responsiveness to PCV13 (for example, for *NCAMI*, $R = -0.82$ and $P = 0.00038$) but not responsiveness to PPSV23 (Fig. 3f). In addition, on average, PBMCs from men showed higher expression of CYTOX genes than PBMCs from women in both cohorts (Fig. 3g and Supplementary Table 6a). Expression levels of the top CYTOX genes increased with age, albeit not significantly (Fig. 3h); age-related upregulation of these genes was also observed in a larger cohort ($n = 41$ men and 34 women; $P < 0.05$ (ref. 27); Extended Data Fig. 6b). A different module (dark green, 134 genes) was specifically associated with reduced PPSV23 responses ($P = 0.05$; Extended Data Fig. 6a,c and Supplementary Table 6b), including genes

associated with the cell cycle and transcriptional regulation (*ANGEL2*, *MRE11*, *MTERF1*, *NUPI07* and *YTHDC2*); however, they were not associated with any immune cell type or function. The top genes in this module showed no significant association with age and sex (Extended Data Fig. 6d,e). To summarize, WGCNA of the baseline PBMC RNA-seq data revealed two distinct gene sets that are significantly associated with PCV13 and PPSV23 responses.

The CYTOX signature stems from CD16⁺ NK cells

To identify cells bearing the CYTOX signature, we generated single-cell RNA-seq (scRNA-seq) data from prevaccination PBMCs of 11 PCV13 donors (6 SRs and 5 WRs), resulting in 52,702 cells after quality control (Fig. 4a and Supplementary Table 7). Clustering of PBMCs generated 24 clusters, which were annotated into monocytes (CD14 and CD16), DCs (monocyte-derived DCs, cDC1s and cDC2s), B cells (naive cells, memory cells, switched memory B cells, age-associated B cells and plasma cells), CD4⁺ T cells (naive, memory, regulatory T (T_{reg}) and cytotoxic CD4⁺ T cells), CD8⁺ T cells (naive and memory cells (granzyme K⁺ T cells, effector memory T cells expressing CD45RA (TEMRA), mucosal-associated invariant T cells and $\gamma\delta$ T cells)) and NK cells (CD56^{bright}CD16⁺ and CD56^{dim}CD16⁺; Fig. 4a and Extended Data Fig. 7a,b). Among these, only two cell subsets were significantly different between SRs and WRs (Fig. 4b and Extended Data Fig. 8a), where SRs had more naive CD8⁺ T cells ($P = 0.03$) and fewer CD16⁺ NK cells ($P = 0.03$; Fig. 4b and Extended Data Fig. 8a).

Blood NK cells include immature CD56^{bright}CD16⁺ NK cells that produce the chemokine XCL1 and the mature, highly cytotoxic CD56^{dim}CD16⁺ cells, both of which were captured in the scRNA-seq data (Fig. 4c). However, only the CD16⁺ NK cells were significantly associated with vaccine responsiveness, where WRs had higher frequencies of these cells (Fig. 4d,e and Extended Data Fig. 8b). In line with their stronger PCV13 responses (Fig. 1f), women had lower CD16⁺ NK cell frequencies than men ($P = 0.042$; Fig. 4f). We calculated CYTOX scores at single-cell resolution using the average expression of CYTOX genes. The CYTOX score was highest in the NK cell populations, followed by the cytotoxic CD8⁺ T cell populations (Extended Data Fig. 9a). There was no significant difference between the CYTOX scores of SRs and WRs neither for the memory CD4⁺ T cell clusters (Extended Data Fig. 9b–e) nor for other cell types, including TEMRAs that have high CYTOX scores (Extended Data Fig. 9e). Together, these data establish that CD16⁺ NK cells comprise the population of cells that bears the CYTOX signature, where the increased frequency of CD16⁺ NK cells is associated with reduced PCV13 responses.

Differential gene expression analyses between CD16⁺ NK cells of SRs and WRs revealed 38 differentially expressed genes (FDR of 5%; Fig. 5a and Supplementary Table 8). CD16⁺ NK cells from WRs showed higher expression of cytotoxic genes (*GZMY* and *GZMH*) and *IFNG*, indicating a more ‘cytotoxic’ and ‘activated’ phenotype. Furthermore, WR CD16⁺ NK cells expressed higher levels of the inhibitory receptor gene *KLRC2* (*NRG2C*), suggesting a more advanced maturation stage²⁸. CD16⁺ NK cells from WRs also overexpressed amphiregulin (*AREG*), a ligand for the epidermal growth factor receptor that is upregulated after

inflammation and mitochondrial stress in immune cells²⁹. Although CMV can modulate NK cell phenotypes³⁰, CMV positivity (10 of 39 donors) was not associated with responsiveness to either vaccine (Fig. 5b). These data suggest that CD16⁺ NK cells from PCV13 WRs had a more cytotoxic and activated transcriptional phenotype than the same cells from SRs.

PPSV23 responses are independent of CD16⁺ NK cell frequency

To establish whether CD16⁺ NK cells are also associated with PPSV23 responsiveness, we used CIBERSORTx and inferred cell-type frequency from bulk data by using cell-type-specific expression from scRNA-seq data (Fig. 4a). First, we confirmed that inferred CD16⁺ NK cell frequencies match scRNA-seq-based frequencies using 11 donors for whom we have both scRNA-seq and bulk PBMC RNA-seq data ($R = 0.97$, $P = 5.4 \times 10^{-6}$; Fig. 5c and Extended Data Fig. 10a). In the PCV13 cohort, inferred CD16⁺ NK cell frequency significantly correlated with responsiveness ($R = -0.69$, $P = 0.0067$), reinforcing our observation. By contrast, the CD16⁺ NK cell frequency was not associated with PPSV23 responsiveness ($R = -0.094$, $P = 0.73$; Fig. 5d and Extended Data Fig. 10b). Together with the lack of association between CYTOX genes and PPSV23 responsiveness (Fig. 3e), these analyses established that CD16⁺ NK cells are important only for responses to the conjugated PCV13 vaccine. Notably, donors with higher CD16⁺ NK cell frequencies also had higher T_H17 cell frequencies ($R = 0.86$, $P = 0.00067$) and lower T_H1 cell frequencies ($R = -0.72$, $P = 0.012$; Fig. 5e), which was not observed for CD16⁺ NK cells (Extended Data Fig. 10c).

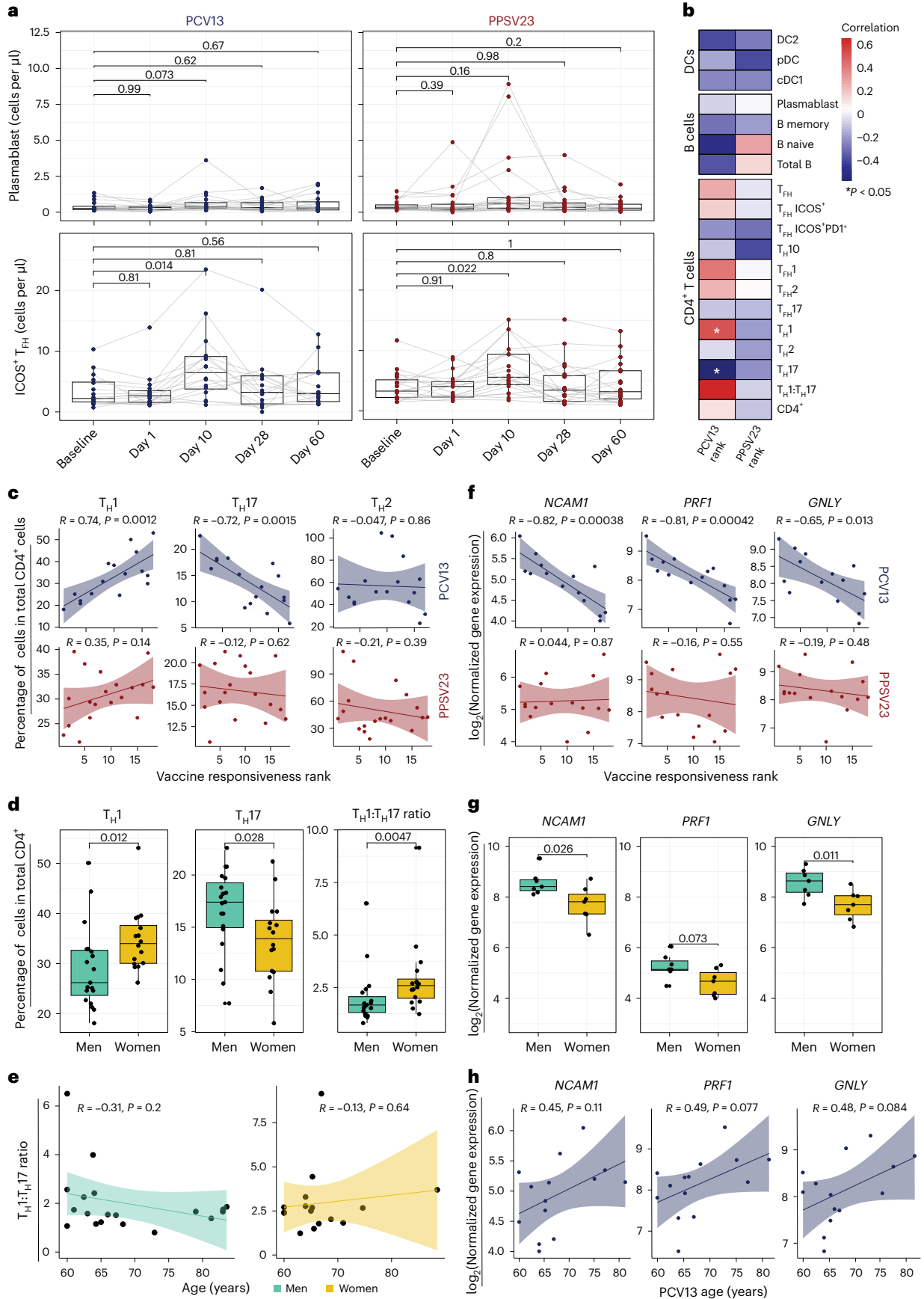
To study the role of CD16⁺ NK cells in responses to other vaccines in older adults, we reanalyzed bulk PBMC RNA-seq data from the previously published Fluzone study ($n = 16$, 65+ years old)³¹. CIBERSORTx-inferred CD16⁺ NK cell frequencies did not show significant differences between responders and non-responders ($P = 0.22$; Fig. 5f). However, reanalyses of scRNA-seq data from individuals treated with the adjuvanted influenza vaccine Fluad ($n = 6$, 65 years old)³² showed that CD16⁺ NK cell frequencies were higher in non-responders than in responders (three responders and three non-responders; $P = 0.072$; Fig. 5f). Together, these data suggest that the CD16⁺ NK cell phenotype and the CYTOX signature are specifically associated with the conjugated pneumococcal vaccine PCV13. Furthermore, the CYTOX signature might also be predictive of responses for other vaccines (for example, Fluad) and might provide an effective strategy for precision vaccinology among older adults (Fig. 5g). Associations between this signature and other vaccines should be studied further in larger cohorts.

Excluding non-informative donors strengthens baseline associations

Previous studies of pneumococcal vaccines showed that donors with high baseline antibody levels have lower fold increases after vaccination³³ (Extended Data Fig. 2a,b). Such donors are likely already protected and can confound conclusions related to vaccine responsiveness and efficacy. However, identification of non-informative (high baseline) donors is particularly challenging for bacterial pneumonia vaccines due to the variability in serotype baselines; some

Fig. 3 | Baseline T_H1:T_H17 cell ratio and cytotoxic gene expression are predictive of PCV13 vaccine responsiveness rank. **a**, Longitudinal analysis of the absolute numbers of plasmablasts (cells per μ l; top) and ICOS⁺ T_H1 cells (cells per μ l; bottom) among the memory CD4⁺ T cell population in response to PCV13 ($n = 16$) and PPSV23 ($n = 19$). **b**, Correlation analysis between the absolute number of different cell types (DC, B cell and CD4⁺ T cell subsets) analyzed in whole blood and ranks. **c**, Correlation analysis between ranks and frequencies of T_H1, T_H17 and T_H2 cells evaluated at baseline. **d**, Sex differences in the frequencies of T_H1 and T_H17 cells and T_H1:T_H17 cell ratio at baseline ($n = 16$ for PCV13; $n = 19$ for PPSV23). T_H1 and T_H17 cell frequencies were calculated relative to the total CD4⁺ T cell count. **e**, Association between T_H1:T_H17 cell ratio and age among men (green) and women (dark yellow) in response to PCV13 and PPSV23. **f**, Correlation analysis between

baseline expression of cytotoxic genes (*NCAMI*, *GZMY* and *PRFI*) and PCV13 vaccine responsiveness rank (top; $n = 14$) and PPSV23 vaccine responsiveness rank (bottom; $n = 16$). **g**, Sex differences in the expression of *NCAMI*, *PRFI* and *GZMY* at baseline ($n = 14$ for PCV13; $n = 16$ for PPSV23). **h**, Association between *NCAMI*, *PRFI* and *GZMY* expression and age ($n = 14$ for PCV13; $n = 16$ for PPSV23). Box plots display the median and IQR (25–75%), with whiskers representing the upper and lower quartiles $\pm 1.5 \times$ IQR. A Wilcoxon matched-pairs signed-rank test (two sided) was used to compare the absolute numbers of plasmablasts and ICOS⁺ T_H1 cells longitudinally (**a**). Correlation analyses were performed using the Pearson correlation metric (**b**, **c**, **e**, **f** and **h**), and P values were computed using two-sided t -tests; n represents the number of biological replicates.



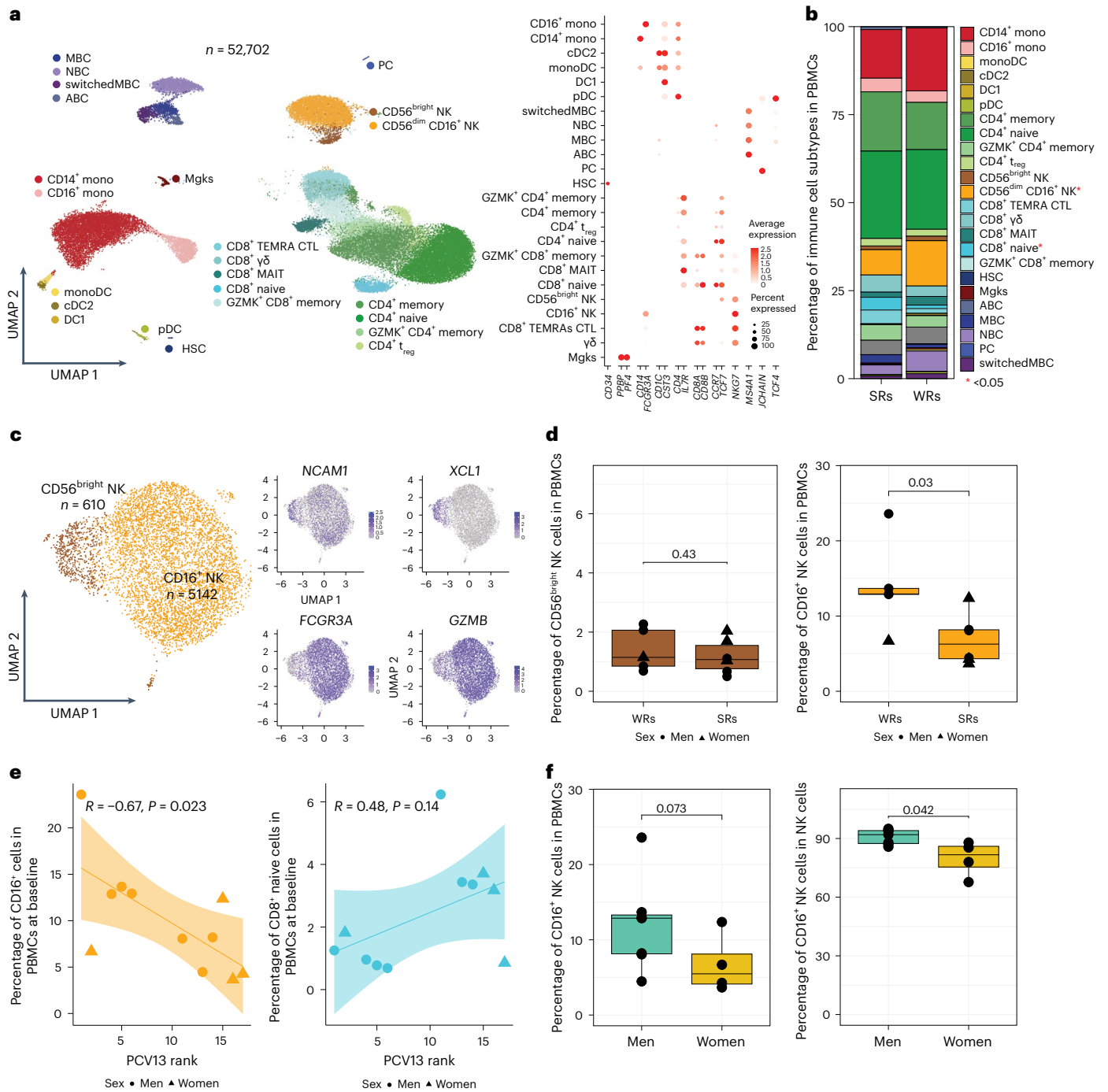


Fig. 4 | CD16⁺ NK cell frequency in PBMCs is negatively associated with PCV13 vaccine responses. **a**, Uniform manifold approximation and projection (UMAP) of PBMCs from 11 PCV13 donors (six SRs and five WRs) showing 24 clusters from 52,702 cells colored by immune cell type. Immune subsets were identified in a supervised manner. Lineage markers are shown in the dot plot; MBC, memory B cell; NBC, naive B cell; ABC, age-associated B cell; mono, monocyte; monoDC, monocyte-derived DC; HSC, hematopoietic stem cell; Mkg, megakaryocyte; MAIT, mucosal-associated invariant T cell; GZMK, granzyme K; PC, plasma cells; CTL, cytotoxic T cell. **b**, Stacked bar plot of immune cell frequencies in SRs and WRs. The cell types with significant differences in their frequencies between SRs and WRs are marked with a red asterisk (*; $P < 0.05$). **c**, UMAP of NK cell subsets with feature plots showing the expression *NCAM1*, *XCL1*, *FCGR3A* and

GZMB in blue, highlighting the two NK populations: CD56^{dim}CD16⁺ NK cells and CD56^{bright} NK cells. **d**, Box plots of CD16⁺ NK cell and CD56^{bright} NK cell frequencies in SRs ($n = 6$) and WRs ($n = 5$). **e**, Correlation analysis between PCV13 rank and prevaccination frequencies of CD16⁺ NK and CD8⁺ naive T cells ($n = 11$). **f**, Sex differences in the prevaccination percentages of CD16⁺ NK cells in total PBMCs and in total NK cells ($n = 11$). Box plots display the median and IQR (25–75%), with whiskers representing the upper and lower quartiles $\pm 1.5 \times$ IQR. A Wilcoxon rank-sum test (two sided) was used to compare cell percentages between SRs and WRs (**b** and **d**) and CD16⁺ NK cell percentages between men and women (**f**). Correlations were computed using the Pearson correlation metric (**e**), and P values were computed using two-sided t -tests; n represents the number of biological replicates.

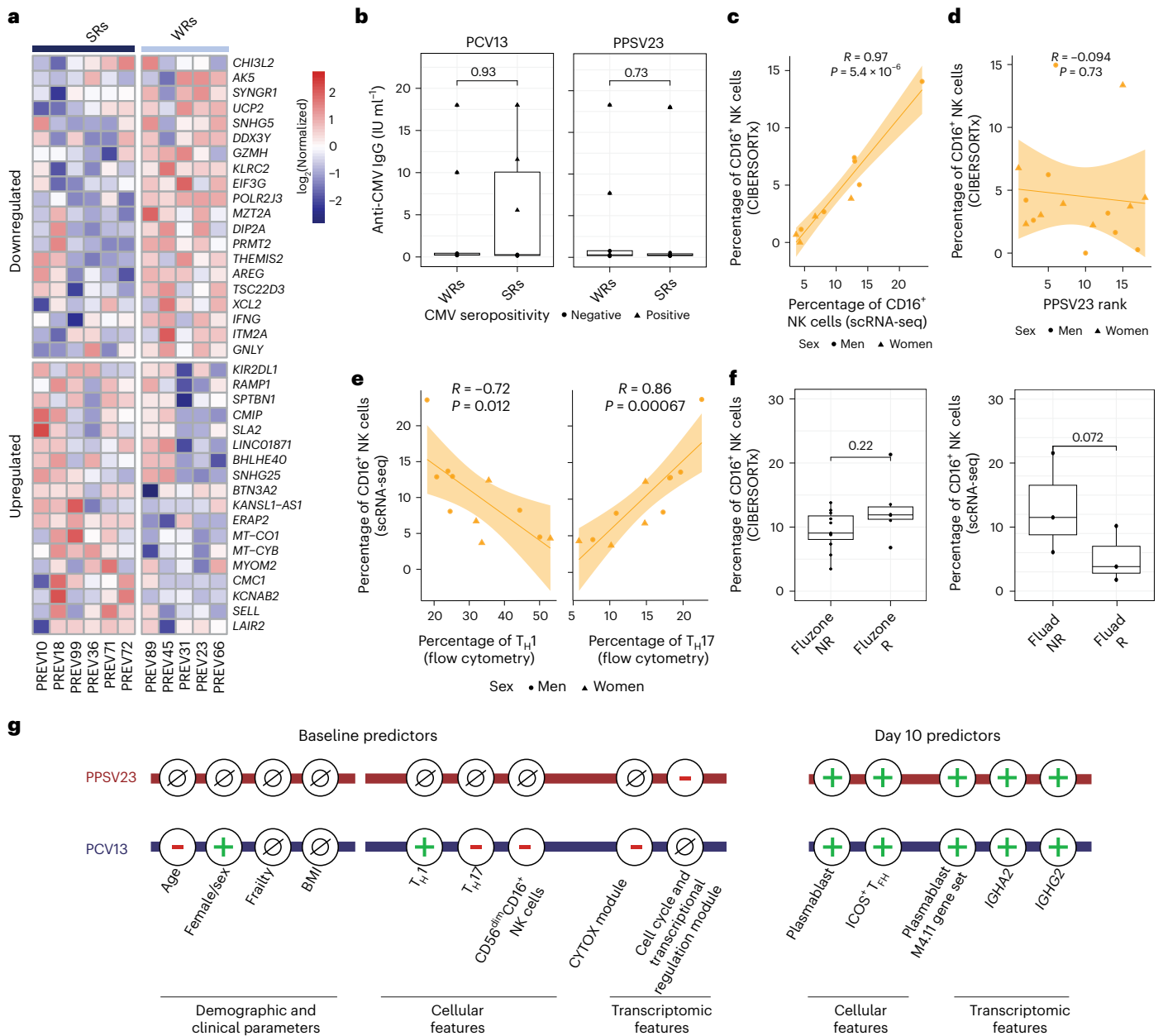


Fig. 5 | Increased cytotoxicity in CD16⁺ NK cells of PCV13 WRs. **a**, Heat map of the differentially expressed genes in CD16⁺ NK cells of six PCV13 SRs and five WRs at baseline, as assessed using normalized expression values from the scRNA-seq pseudobulk analysis. **b**, Box plots comparing anti-CMV IgG titers between SRs and WRs for PCV13 (left) and PPSV23 (right). **c**, Correlation analysis of prevaccination CD16⁺ NK cell percentages estimated by scRNA-seq and CIBERSORTx ($n = 11$). **d**, Correlation analysis of CIBERSORTx-based estimates of CD16⁺ NK cells and PPSV23 rank ($n = 16$) at baseline. **e**, Correlation analysis of CD16⁺ NK cell percentages determined by scRNA-seq and T_{H1} and T_{H17} cell percentages determined using flow cytometry at baseline. **f**, Box plots of prevaccination CD16⁺ NK cell percentages in Fluad responders (R; $n = 3$) and non-responders

(NR; $n = 3$) and Fluzone trivalent inactivated influenza vaccine responders ($n = 5$) and non-responders ($n = 11$). **g**, Summary schema showing the demographic, clinical, cellular and transcriptomic parameters associated with PCV13 and PPSV23 vaccine responsiveness at baseline and day 10. Box plots display the median and IQR (25–75%), with whiskers representing the upper and lower quartiles $\pm 1.5 \times$ IQR. A Wilcoxon rank-sum test (two sided) was used to compare the mean anti-CMV IgG titers between SRs and WRs of PCV13 and PPSV13 donors (**b**) and prevaccination CD16⁺ NK cell percentages in Fluad responders and non-responders and Fluzone responders and non-responders (**f**). Correlation analyses were computed using the Pearson correlation metric (**c**, **d** and **e**), and P values were computed using two-sided t -tests; n represents the number of biological replicates.

serotypes have consistently higher baselines (9V, 19A and 19F in our cohort; Fig. 6a) due to the variability in baseline titer levels among different cohorts²³. To overcome this, we previously developed an analytical strategy to bin donors into three groups: SRs (low baseline, high fold increase in titers), WRs (low baseline, low fold increase) and non-informative donors (high baseline titers)²³. Using this strategy, we identified 10 SRs, 6 WRs and 3 non-informative donors in the PCV13

arm and 11 SRs, 7 WRs and 2 non-informative donors in the PPSV23 arm (Supplementary Table 9a,b).

We excluded the non-informative donors and repeated all the analyses, which confirmed and, in some instances, strengthened all the associations observed with vaccine responsiveness. In summary, there was a significant age-related decline in responsiveness to both PCV13 ($R = -0.7$, $P = 0.0026$) and PPSV23 ($R = -0.47$, $P = 0.047$) vaccines (Fig. 6b

and Supplementary Table 9c,d). Women mounted stronger responses to PCV13 than men across the three metrics strength ($P = 0.012$), extent ($P = 0.033$) and rank ($P = 0.026$; Fig. 6c and Supplementary Table 9c), which was not observed for PPSV23 (Supplementary Table 9d). Baseline frequencies of T_{H1} ($R = 0.72, P = 0.0015$) and T_{H17} ($R = -0.73, P = 0.0013$) cells correlated with PCV13 responses (Fig. 6d) but not with PPSV23 responses. The baseline CYTOX module score and expression of its top genes (*NCAMI*, *GPLY* and *PRFI*) were negatively associated specifically with PCV13 responses ($R = -0.65, P = 0.0023$; Fig. 6e). Moreover, men showed higher expression of CYTOX genes than women (Supplementary Table 9c). Finally, PCV13 WRs had higher baseline frequencies of $CD16^+$ NK cells than SRs ($P = 0.024$; Fig. 6f). The dark green module score and baseline expression of its top genes (*ANGEL2* and *ZNF529*) negatively correlated specifically with PPSV23 responses (Supplementary Table 9d). These new analyses suggest that, even among pneumococcal vaccine-naïve older adults, 10–15% of the cohort have high baseline titers. The demographic, baseline cellular and transcriptional features associated with responsiveness to PCV13 and PPSV23 are independent of these non-informative donors.

Discussion

Older adults are at high risk for morbidity and mortality due to infectious diseases¹, including those caused by *S. pneumoniae*. Despite the availability of two types of FDA-approved pneumococcal vaccines, responsiveness of older adults to these vaccines remains poorly characterized. We studied the responses of 39 older adults to PPSV23 or conjugated PCV13 and uncovered (1) strong antibody responses to both vaccines and transcriptional activation of plasmablast genes at day 10, (2) increased ICOS⁺ T_{FH} cells at day 10 for both vaccines, (3) a baseline immune phenotype composed of increased frequencies of T_{H17} cells, reduced frequencies of T_{H1} cells and increased frequencies of $CD16^+$ NK cells that is specifically associated with PCV13 responses and is more frequently observed in men than in women and (4) a distinct baseline gene expression module that is associated with PPSV23 responses.

Both vaccines induced strong antibody responses, although PCV13 induced higher increases in OPA titers than PPSV23, in line with observations in younger adults³⁴. Both vaccines induced strong responses to the 12 shared serotypes. Although PPSV23 lacks serotype 6A, some donors showed increased antibody responses to this serotype, potentially due to the cross-reactivity with serotype 6B. The strongest transcriptional signal was the upregulation of plasmablast genes, in particular immunoglobulins, at day 10. Both vaccines predominantly induced the expression of the heavy chain constant region genes encoding IgG2 and IgA2 isotypes, distinct from influenza vaccine responses (IgG1 and IgG3). A recent study on PCV13 and PPSV23 (ref. 24) showed an increased abundance of these isotypes 30 d after vaccination with either vaccine. Despite the strong transcriptional upregulation of plasmablast genes at day 10, increases in the numbers of circulating plasmablasts were marginal. It is possible that 10 d after vaccination was not the ideal time point to detect peak plasmablast responses or the responses were weaker in older adults. Indeed, in a previous study, we showed that, after PCV13 vaccination¹¹, antigen-specific (AIM⁺) T_{FH} cells were expanded in younger donors but not in older donors.

The release of plasma cells into circulation is linked to the frequencies of activated T_{FH} cells that positively correlate with serological responses to influenza vaccine and are affected by aging³⁵. For pneumococcal vaccines, there was a significant expansion of ICOS⁺ T_{FH} cells at day 10; however, this expansion did not correlate with antibody responses, which could be due to age of our donors or the timing of our T_{FH} measurement (day 10 versus day 7). The expansion of ICOS⁺ T_{FH} cells in response to PPSV23 (at comparable levels to PCV13) suggests that PPSV23 also induces T cell immunity. A lower frequency of T_{H1} cells and higher frequency of T_{H17} cells at baseline was associated with weaker responses to PCV13. Age-dependent increases in T_{H17} cells or increased production of IL-17 have been observed^{36,37}. The frequencies of these cell types were not significantly associated with age, although a significant sex association was observed. Women had higher T_{H1} and lower T_{H17} cell frequencies than age-matched men, which might explain their stronger responses to PCV13. Proinflammatory molecules (IL-6 and IL-1 β) that promote T_{H17} cell differentiation³⁸ are also linked to systemic chronic inflammation with aging (that is, inflammaging)³⁹. Accelerated inflammaging in men²⁷ might contribute to the observed sex differences in PCV13 responses. In contrast to our previous study in young adults¹⁹, we did not detect an innate response at day 1 for either vaccine due to the already elevated myeloid signatures in older individuals or to an age-specific altered response to these vaccines.

The cell types uncovered here (T_{H17} , T_{H1} and $CD16^+$ NK cells) go through significant age-related changes. Although the global proportion of T_{H17} cells among memory $CD4^+$ T cells declines with age⁴⁰, a significant increase in the T_{H17} : T_{reg} cell ratio was observed in older individuals³⁶. Additionally, when activated in vitro, $CD4^+$ naive T cells from older individuals show enhanced T_{H17} differentiation compared to $CD4^+$ naive T cells from younger individuals. The proportion of NK cells among peripheral blood lymphocytes increases with age^{41–43}. Our study shows that a higher proportion of $CD16^+$ NK cells is associated with worse responses to PCV13 in older individuals, highlighting the significance of NK cell aging in the context of age-associated decline in vaccine responses.

Baseline bulk RNA-seq data revealed a cytotoxicity-associated gene set (CYTOX) that predicted reduced responses to conjugated PCV13, and scRNA-seq data indicated that this CYTOX signature stems from mature $CD16^+$ NK cells that are more cytotoxic and have antibody-dependent cellular cytotoxicity functions²⁶. Although antibody-dependent cellular cytotoxicity-proficient antibody production is a key correlate of vaccine responses, including for bacterial pneumonia vaccines²⁴, activated NK cells might be detrimental for vaccine responses. For the yellow fever vaccine YF-17D, the frequency of activated NK cells at day 7 was linked to reduced neutralizing antibody levels⁴⁴. For malaria vaccines, blood transcriptional modules associated with NK cells displayed a strong negative correlation with antibody response and protection at multiple time points⁴⁵.

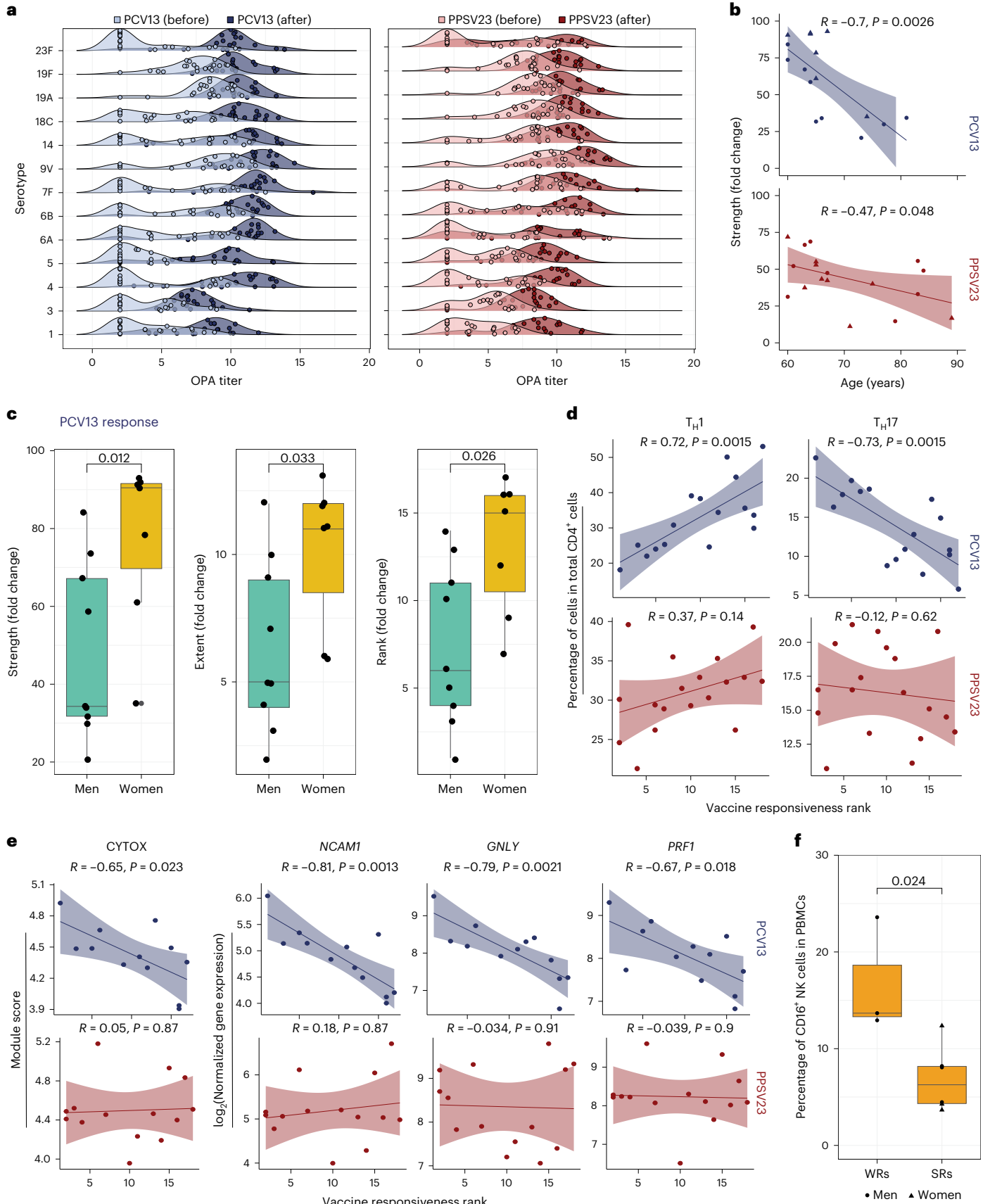
$CD16^+$ NK cells from WRs expressed cytotoxicity-related genes at higher levels than those from SRs. These cytotoxic molecules and some NK receptors are also upregulated with age in $CD8^+$ TEMRA cells, which was captured in the scRNA-seq data yet was not associated with PCV13 responses. Interestingly, $CD16^+$ NK cell frequency significantly

Fig. 6 | Association between demographic, cellular and transcriptomic parameters and vaccine responsiveness after the exclusion of non-informative donors. **a**, Ridge plot displaying the distribution of before and after vaccination OPA titers for each serotype in the PCV13 ($n = 19$) and PPSV23 ($n = 20$) cohorts. Note that baseline titer levels vary among serotypes. Non-informative donors were identified using a published strategy, and associations were recalculated after exclusion of these donors. **b**, Association between PCV13 ($n = 16$) and PPSV23 ($n = 18$) strength and age (in years). **c**, Sex differences in PCV13 ($n = 16$) and PPSV23 ($n = 18$) vaccine responses. Note that women mount significantly stronger responses to the PCV13 vaccine. **d**, Association between T_{H1} and T_{H17} cell percentages at baseline and PCV13 ($n = 15$) and PPSV23 ($n = 17$)

vaccine responsiveness. **e**, Correlations between CYTOX scores at baseline and PCV13 ($n = 12$) and PPSV23 ($n = 14$) vaccine responsiveness (left) and correlations between the baseline expression of *NCAMI*, *GPLY* and *PRFI* and PCV13 and PPSV23 vaccine responsiveness (right). **f**, Baseline abundance of $CD16^+$ NK cells in PCV13 SRs ($n = 6$) and WRs ($n = 3$). Correlation analyses were computed using the Pearson correlation metric (**b** and **d–f**), and P values were computed by using two-sided t -tests. Box plots display the median and IQR (25–75%), with whiskers representing the upper and lower quartiles $\pm 1.5 \times$ IQR. A Wilcoxon rank-sum test (two sided) was used to compare strength, extent and rank between men and women treated with PCV13 and PPSV23 (**c**); n represents the number of biological replicates.

correlated with T_H cell subsets associated with PCV13 responses. Donors who had higher frequencies of CD16⁺ NK cells had higher T_H17 cell frequencies and lower T_H1 cell frequencies. Whether this reflects a

parallel co-regulation of these three subsets in older donors or whether CD16⁺ NK cells contribute to the imbalance of T_H1 and T_H17 cells remains to be established. The role of NK cells in modulating T cells has been



explored in autoimmunity, transplantation, pregnancy and infection^{46–50}. These studies concluded that NK cells can modulate T_H17 and T_H1 cell expansion via IL-17A or interferon- γ secretion or by direct killing of activated helper T cells. Additionally, helper T cell killing by NK cells is sensitive to helper T cell-secreted IL-2 quantity and helper T cell expression of HLA-E (inhibitory) or NKG2D or DNAM-1 ligands (stimulatory). Mouse studies showed that NK cells can kill helper T cells and T_{FH} cells in certain viral infection settings, resulting in worse cytotoxic T cell responses and reduced germinal center formation, B cell affinity maturation and neutralizing antibody titers^{46,51–54}. Indeed, NK cell depletion before vaccination increased vaccine-induced antibody responses in mice⁵³.

Capsular polysaccharidic antigens in pneumococcal vaccines can neutralize preexisting antibodies or paralyze B cells, potentially rendering a vaccine more susceptible to infections^{55–57}. This could, in theory, contribute to an increased incidence of pneumonia (although not death) in vaccinated older adults. However, pneumococcal conjugated vaccines are shown to be effective in preventing invasive disease in older adults⁵⁸ and in human immunodeficiency virus (HIV)-infected adults⁵⁹. In agreement, a meta-analysis of 18 randomized trials ($n = 64,500$ donors) showed that pneumococcal polysaccharide vaccines reduce the risk of both invasive and noninvasive pneumococcal disease⁶⁰.

Here, we present a precision vaccinology study of pneumococcal vaccine responses in older adults. Remarkably, the baseline predictors for the two vaccines were distinct, despite that both vaccines include the same polysaccharidic antigens. Our study provides a framework for stratification of older adults for the administration of pneumococcal vaccines, with potential implications for other vaccines, by establishing blood-based clinical assays to assess whether an individual has the CYTOX signature (for example, by quantifying the expression of *NCAM1* by using quantitative real-time PCR or the frequency of CD16⁺ NK cells by using flow cytometry). As the CYTOX signature only affects responsiveness to PCV13, donors with a high CYTOX signature likely benefit from PPSV23, whereas donors with a low CYTOX signature likely benefit from PCV13. Future studies are needed to establish whether these baseline signatures are also predictive in other populations. Our data also show the importance of biological sex for vaccine administration; women had stronger responses to conjugated PCV13 as they had lower CYTOX activity than age-matched men. These findings might also yield novel strategies to change baseline immune phenotypes to alter vaccine responses^{61,62}, for example, by temporarily blocking the immunosuppressive or cytolytic functions of CD16⁺ NK cells before vaccination⁶³. Strategies such as activating receptor blockade or epigenetic remodeling of NK cell effector functions hold potential for modulating NK cell cytotoxicity. However, these strategies are still in their infancy, and their safety and cell-type specificity are not clear.

Study limitations

We acknowledge several limitations of our study. First, due to the frequency of the early visits, we collected blood at day 10 to study adaptive responses, which might miss the peak adaptive responses. Future longitudinal studies should investigate adaptive responses of older adults at additional time points. Second, we used OPA assays to quantify vaccine responses because they (1) mimic functional immune responses, (2) are considered state of the art for FDA approvals and (3) are more effective than ELISAs among older adults²¹. However, this decision came at a cost, and we did not have enough material to quantify OPA titers for all 23 serotypes. We therefore prioritized the most prevalent 13, which are the ones selected for the PCV13 vaccine formulation^{22,64}. Although our quantification for PPSV23 closely captures donor protection from the most prevalent serotypes and is a good proxy for overall responsiveness, it does not fully capture the immune responses to all 23 serotypes. Third, due to limitations in material, we could not study the B and T cell memory responses in depth (that is, antigen-specific

cells and their responses). Future studies are needed to further explore B and T cell responses of older adults to these vaccines.

Online content

Any methods, additional references, Nature Portfolio reporting summaries, source data, extended data, supplementary information, acknowledgements, peer review information; details of author contributions and competing interests; and statements of data and code availability are available at <https://doi.org/10.1038/s41590-023-01717-5>.

References

- Huang, S. S. et al. Healthcare utilization and cost of pneumococcal disease in the United States. *Vaccine* **29**, 3398–3412 (2011).
- Daniels, C. C., Rogers, P. D. & Shelton, C. M. A review of pneumococcal vaccines: current polysaccharide vaccine recommendations and future protein antigens. *J. Pediatr. Pharmacol. Ther.* **21**, 27–35 (2016).
- Weller, S. et al. Human blood IgM ‘memory’ B cells are circulating splenic marginal zone B cells harboring a prediversified immunoglobulin repertoire. *Blood* **104**, 3647–3654 (2004).
- Weller, S. et al. T-independent responses to polysaccharides in humans mobilize marginal zone B cells prediversified against gut bacterial antigens. *Sci. Immunol.* **8**, eade1413 (2023).
- Douglas, R. M., Paton, J. C., Duncan, S. J. & Hansman, D. J. Antibody response to pneumococcal vaccination in children younger than five years of age. *J. Infect. Dis.* **148**, 131–137 (1983).
- Timens, W., Boes, A., Rozeboom-Uiterwijk, T. & Poppema, S. Immaturity of the human splenic marginal zone in infancy. Possible contribution to the deficient infant immune response. *J. Immunol.* **143**, 3200–3206 (1989).
- Shi, Y. et al. Regulation of aged humoral immune defense against pneumococcal bacteria by IgM memory B cell. *J. Immunol.* **175**, 3262–3267 (2005).
- Weill, J.-C., Weller, S. & Reynaud, C.-A. Human marginal zone B cells. *Annu. Rev. Immunol.* **27**, 267–285 (2009).
- Clutterbuck, E. A. et al. Pneumococcal conjugate and plain polysaccharide vaccines have divergent effects on antigen-specific B cells. *J. Infect. Dis.* **205**, 1408–1416 (2012).
- Mishra, R. P. N. et al. Structural and immunological characterization of *E. coli* derived recombinant CRM197 protein used as carrier in conjugate vaccines. *Biosci. Rep.* **38**, BSR20180238 (2018).
- Sterrett, S. et al. Peripheral CD4 T follicular cells induced by a conjugated pneumococcal vaccine correlate with enhanced opsonophagocytic antibody responses in younger individuals. *Vaccine* **38**, 1778–1786 (2020).
- Bonten, M. J. M. et al. Polysaccharide conjugate vaccine against pneumococcal pneumonia in adults. *N. Engl. J. Med.* **372**, 1114–1125 (2015).
- Park, S. & Nahm, M. H. Older adults have a low capacity to opsonize pneumococci due to low IgM antibody response to pneumococcal vaccinations. *Infect. Immun.* **79**, 314–320 (2011).
- Jackson, L. A. & Janoff, E. N. Pneumococcal vaccination of elderly adults: new paradigms for protection. *Clin. Infect. Dis.* **47**, 1328–1338 (2008).
- Shelly, M. A. et al. Comparison of pneumococcal polysaccharide and CRM197-conjugated pneumococcal oligosaccharide vaccines in young and elderly adults. *Infect. Immun.* **65**, 242–247 (1997).
- Kraicer-Melamed, H., O'Donnell, S. & Quach, C. The effectiveness of pneumococcal polysaccharide vaccine 23 (PPV23) in the general population of 50 years of age and older: a systematic review and meta-analysis. *Vaccine* **34**, 1540–1550 (2016).

17. Shah, A. A. Simplifying pneumococcal immunizations for adults. *Am. Fam. Physician* **105**, 580–581 (2022).
18. Li, S. et al. Molecular signatures of antibody responses derived from a systems biology study of five human vaccines. *Nat. Immunol.* **15**, 195–204 (2014).
19. Obermoser, G. et al. Systems scale interactive exploration reveals quantitative and qualitative differences in response to influenza and pneumococcal vaccines. *Immunity* **38**, 831–844 (2013).
20. Song, J. Y., Moseley, M. A., Burton, R. L. & Nahm, M. H. Pneumococcal vaccine and opsonic pneumococcal antibody. *J. Infect. Chemother.* **19**, 412–425 (2013).
21. Centers for Disease Control and Prevention (CDC). Licensure of 13-valent pneumococcal conjugate vaccine for adults aged 50 years and older. *MMWR Morb. Mortal. Wkly. Rep.* **61**, 394–395 (2012).
22. Burton, R. L. & Nahm, M. H. Development and validation of a fourfold multiplexed opsonization assay (MOPA4) for pneumococcal antibodies. *Clin. Vaccin. Immunol.* **13**, 1004–1009 (2006).
23. LaFon, D., Kim, Y., Burton, R., Dransfield, M. & Nahm, M. Pneumococcal antibody function for immunologic evaluation: normal results in older adults, and a novel analytical model for vaccine response. *J. Clin. Immunol.* **41**, 1964–1968 (2021).
24. Davies, L. R. L. et al. Polysaccharide and conjugate vaccines to *Streptococcus pneumoniae* generate distinct humoral responses. *Sci. Transl. Med.* **14**, eabm4065 (2022).
25. Bentebibel, S.-E. et al. Induction of ICOS⁺CXCR3⁺CXCR5⁺ T_H cells correlates with antibody responses to influenza vaccination. *Sci. Transl. Med.* **5**, 176ra32 (2013).
26. Liu, X. & Lieberman, J. Knocking'em dead: pore-forming proteins in immune defense. *Annu. Rev. Immunol.* **38**, 455–485 (2020).
27. Márquez, E. J. et al. Sexual-dimorphism in human immune system aging. *Nat. Commun.* **11**, 751 (2020).
28. Perera Molligoda Arachchige, A. S. Human NK cells: from development to effector functions. *Innate Immun.* **27**, 212–229 (2021).
29. Zaiss, D. M. W., Gause, W. C., Osborne, L. C. & Artis, D. Emerging functions of amphiregulin in orchestrating immunity, inflammation, and tissue repair. *Immunity* **42**, 216–226 (2015).
30. Kuijpers, T. W. et al. Human NK cells can control CMV infection in the absence of T cells. *Blood* **112**, 914–915 (2008).
31. Thakar, J. et al. Aging-dependent alterations in gene expression and a mitochondrial signature of responsiveness to human influenza vaccination. *Aging* **7**, 38–52 (2015).
32. Riese, P. et al. Distinct immunological and molecular signatures underpinning influenza vaccine responsiveness in the elderly. *Nat. Commun.* **13**, 6894 (2022).
33. Hare, N. D., Smith, B. J. & Ballas, Z. K. Antibody response to pneumococcal vaccination as a function of preimmunization titer. *J. Allergy Clin. Immunol.* **123**, 195–200 (2009).
34. Jackson, L. A. et al. Immunogenicity and safety of a 13-valent pneumococcal conjugate vaccine compared to a 23-valent pneumococcal polysaccharide vaccine in pneumococcal vaccine-naïve adults. *Vaccine* **31**, 3577–3584 (2013).
35. Herati, R. S. et al. Vaccine-induced ICOS⁺CD38⁺ circulating T_{FH} are sensitive biosensors of age-related changes in inflammatory pathways. *Cell Rep. Med.* **2**, 100262 (2021).
36. Schmitt, V., Rink, L. & Uciechowski, P. The T_H17/T_{reg} balance is disturbed during aging. *Exp. Gerontol.* **48**, 1379–1386 (2013).
37. Bharath, L. P. et al. Metformin enhances autophagy and normalizes mitochondrial function to alleviate aging-associated inflammation. *Cell Metab.* **32**, 44–55 (2020).
38. Kimura, A. & Kishimoto, T. IL-6: regulator of T_{reg}/T_H17 balance. *Eur. J. Immunol.* **40**, 1830–1835 (2010).
39. Franceschi, C. & Campisi, J. Chronic inflammation (inflammaging) and its potential contribution to age-associated diseases. *J. Gerontol. A Biol. Sci. Med. Sci.* **69**, S4–S9 (2014).
40. Lee, J. S. et al. Age-associated alteration in naive and memory T_H17 cell response in humans. *Clin. Immunol.* **140**, 84–91 (2011).
41. Gounder, S. S. et al. Effect of aging on NK cell population and their proliferation at ex vivo culture condition. *Anal. Cell. Pathol.* **2018**, 7871814 (2018).
42. Chidrawar, S. M., Khan, N., Chan, Y. L. T., Nayak, L. & Moss, P. A. Ageing is associated with a decline in peripheral blood CD56^{bright} NK cells. *Immun. Ageing* **3**, 10 (2006).
43. Le Garff-Tavernier, M. et al. Human NK cells display major phenotypic and functional changes over the life span. *Aging Cell* **9**, 527–535 (2010).
44. Muyanja, E. et al. Immune activation alters cellular and humoral responses to yellow fever 17D vaccine. *J. Clin. Invest.* **124**, 3147–3158 (2014).
45. Kazmin, D. et al. Systems analysis of protective immune responses to RTS,S malaria vaccination in humans. *Proc. Natl Acad. Sci. USA* **114**, 2425–2430 (2017).
46. Ali, A. et al. Natural killer cell immunosuppressive function requires CXCR3-dependent redistribution within lymphoid tissues. *J. Clin. Invest.* **131**, e146686 (2021).
47. Arbelaez, C. A., Palle, P., Charaix, J. & Bettelli, E. STAT1 signaling protects self-reactive T cells from control by innate cells during neuroinflammation. *JCI Insight* **7**, e148222 (2022).
48. Fu, B. et al. Natural killer cells promote immune tolerance by regulating inflammatory T_H17 cells at the human maternal-fetal interface. *Proc. Natl Acad. Sci. USA* **110**, E231–E240 (2013).
49. Li, J. et al. Natural killer cells regulate T_H1/T_{reg} and T_H17/T_{reg} balance in chlamydial lung infection. *J. Cell. Mol. Med.* **20**, 1339–1351 (2016).
50. Pallmer, K. & Oxenius, A. Recognition and regulation of T cells by NK cells. *Front. Immunol.* **7**, 251 (2016).
51. Rydzynski, C. E. et al. Affinity maturation is impaired by natural killer cell suppression of germinal centers. *Cell Rep.* **24**, 3367–3373 (2018).
52. Rydzynski, C. et al. Generation of cellular immune memory and B-cell immunity is impaired by natural killer cells. *Nat. Commun.* **6**, 6375 (2015).
53. Reighard, S. D. et al. Therapeutic targeting of follicular T cells with chimeric antigen receptor-expressing natural killer cells. *Cell Rep. Med.* **1**, 100003 (2020).
54. Waggoner, S. N., Cornberg, M., Selin, L. K. & Welsh, R. M. Natural killer cells act as rheostats modulating antiviral T cells. *Nature* **481**, 394–398 (2012).
55. Daum, R. S. et al. Decline in serum antibody to the capsule of *Haemophilus influenzae* type b in the immediate postimmunization period. *J. Pediatr.* **114**, 742–747 (1989).
56. Pichichero, M. E. Immunological paralysis to pneumococcal polysaccharide in man. *Lancet* **2**, 468–471 (1985).
57. French, N. et al. 23-valent pneumococcal polysaccharide vaccine in HIV-1-infected Ugandan adults: double-blind, randomised and placebo controlled trial. *Lancet* **355**, 2106–2111 (2000).
58. Jackson, L. A. et al. Effectiveness of pneumococcal polysaccharide vaccine in older adults. *N. Engl. J. Med.* **348**, 1747–1755 (2003).
59. French, N. et al. A trial of a 7-valent pneumococcal conjugate vaccine in HIV-infected adults. *N. Engl. J. Med.* **362**, 812–822 (2010).
60. Moberley, S., Holden, J., Tatham, D. P. & Andrews, R. M. Vaccines for preventing pneumococcal infection in adults. *Cochrane Database Syst. Rev.* **2013**, CD000422 (2013).
61. Tsang, J. S. et al. Global analyses of human immune variation reveal baseline predictors of post-vaccination responses. *Cell* **157**, 499–513 (2014).

62. Nehar-Belaid, D. et al. Baseline immune states (BIS) associated with vaccine responsiveness and factors that shape the BIS. *Semin. Immunol.* **70**, 101842 (2023).
63. Cox, A. et al. Targeting natural killer cells to enhance vaccine responses. *Trends Pharmacol. Sci.* **42**, 789–801 (2021).
64. Romero-Steiner, S. et al. Use of opsonophagocytosis for serological evaluation of pneumococcal vaccines. *Clin. Vaccin. Immunol.* **13**, 165–169 (2006).

Publisher's note Springer Nature remains neutral with regard to jurisdictional claims in published maps and institutional affiliations.

Open Access This article is licensed under a Creative Commons Attribution 4.0 International License, which permits use, sharing,

adaptation, distribution and reproduction in any medium or format, as long as you give appropriate credit to the original author(s) and the source, provide a link to the Creative Commons license, and indicate if changes were made. The images or other third party material in this article are included in the article's Creative Commons license, unless indicated otherwise in a credit line to the material. If material is not included in the article's Creative Commons license and your intended use is not permitted by statutory regulation or exceeds the permitted use, you will need to obtain permission directly from the copyright holder. To view a copy of this license, visit <http://creativecommons.org/licenses/by/4.0/>.

© The Author(s) 2024

¹The Jackson Laboratory for Genomic Medicine, Farmington, CT, USA. ²UConn Center on Aging, University of Connecticut, Farmington, CT, USA. ³Division of Pulmonary, Allergy and Critical Care Medicine, School of Medicine, University of Alabama at Birmingham, Birmingham, AL, USA. ⁴Drukier Institute for Children's Health and Department of Pediatrics, Weill Cornell Medicine, New York, NY, USA. ⁵Department of Immunology and Microbiology, The Scripps Research Institute, La Jolla, CA, USA. ⁶Institute for Systems Genomics, University of Connecticut Health Center, Farmington, CT, USA. ⁷Department of Genetics and Genome Sciences, University of Connecticut Health Center, Farmington, CT, USA. ⁸Present address: University of Buenos Aires, School of Medicine, Buenos Aires, Argentina. ⁹Present address: Leiden University Medical Center (LUMC), Leiden, the Netherlands. ¹⁰Present address: Immunoledge LLC, Montclair, NJ, USA. ¹¹These authors contributed equally: Sathyabaarathi Ravichandran, Fernando Erra-Diaz, Onur E. Karakaslar. ✉e-mail: duygu.ucar@jax.org

Methods

Participant recruitment

This study was conducted following approval by the UConn Health Center Institutional Review Board (16-071J-1) and registration on ClinicalTrials.gov (NCT03104075). The complete information on clinical trial registration, study protocol, data collection and outcomes can be accessed via <http://clinicaltrials.gov/study/NCT03104075>. All participants provided informed consent and were compensated for their time and study visits. Blood samples were obtained from 39 healthy volunteers residing in the Greater Hartford, CT, region recruited by the UConn Center on Aging Recruitment and Community Outreach Research Core (<http://health.uconn.edu/aging/research/research-cores/>). Volunteers were vaccinated from May to early fall of 2017–2018 to avoid potential overlap with seasonal peak periods of influenza vaccination and infection. None of the participants reported a history of previous pneumonia. Recruitment criteria were selected to identify individuals representing ‘usual healthy’ aging, aligning with the 2019 National Institutes of Health (NIH) Policy on Inclusion Across the Lifespan (NOT-98-024). This selection would increase the generalizability of our study and translate to the general population. Inclusion criteria included an age of 60 years or older and willingness to receive PCV13 (Wyeth/Pfizer) or PPSV23 (Merck) vaccination via random assignment. Exclusion criteria included prior PCV13 or PPSV23 vaccination or a history of adverse reactions to these or any diphtheria toxoid-containing vaccine. Individuals were also excluded if they had a recent fever, received a Zostavax (shingles) vaccine in the previous 4 weeks or had notably confounding comorbidities, such as diabetes mellitus, active malignancy or recurrence in the last 5 years, congestive heart failure, unstable cardiovascular disease in the last 6 months, renal failure, impaired hepatic function, autoimmune diseases (for example, rheumatoid arthritis, lupus and inflammatory bowel disease), recent trauma or surgery, HIV or other immunodeficiency, current substance or alcohol abuse and usage of medications that alter the immune system (for example, prednisone ≥ 10 mg).

Sample collection and PBMC isolation

Thirty-nine donors (20 men and 19 women) were randomly assigned to receive either PCV13 or PPSV23 at the University of Connecticut Health at Farmington, CT. Peripheral blood was collected at baseline (before vaccination at day -7) and after vaccination (days 1, 10, 28 and 60). Data collection and analysis were not performed blind to the conditions of the experiments. Detailed information on participant demographics is provided in Supplementary Table 1a,b. PBMCs were isolated from blood collected in ACD tubes using a Lymphoprep gradient (Stem-Cell Technologies), while serum was isolated from blood collected in red-top collection tubes (BD Vacutainer). Both PBMCs and serum were cryopreserved before subsequent analyses.

OPA titer measurements

Multiplexed opsonization assays were performed for 13 serotypes (1, 3, 4, 5, 6A, 6B, 7F, 9V, 14, 18C, 19A, 19F and 23F) across 39 donors, as previously described²². Frozen aliquots of target pneumococci were thawed, washed twice with Opsonization Buffer B (Hanks’ balanced salt solution with Mg^{2+}/Ca^{2+} , 0.1% gelatin and 10% fetal bovine serum (pH 7.2–7.4)) by centrifugation (12,000g, 2 min) and diluted to the proper bacterial density ($\sim 2 \times 10^5$ colony-forming units per ml of each serotype). Equal volumes of four chosen bacterial suspensions were pooled for analysis. All serum samples were preincubated at 56 °C for 30 min, followed by serial dilutions in Opsonization Buffer B. Serially diluted serum (20 μ l per well) was mixed with 10 μ l of bacterial suspension in each well of a round-bottom 96-well plate.

After a 30-min incubation at 25 °C with shaking at 700 r.p.m. on a mini orbital shaker (Bellco Biotechnology), 10 μ l of 3- to 4-week-old rabbit complement (PelFreeze Biologicals) and 40 μ l of HL60 cells (4×10^5 cells) were added to each well. HL60 cells (ATCC clone CCL-240)

were differentiated to granulocytes by culturing in RPMI-1640 with 10% fetal bovine serum and 1% L-glutamine and 0.8% dimethylformamide at a starting density of 4×10^5 cells per ml for 5–6 d. Plates were incubated in a tissue culture incubator (37 °C, 5% CO₂) with shaking at 700 r.p.m. After a 45-min incubation, plates were placed on ice for 10–15 min, and an aliquot of the final reaction mixture (10 μ l) was spotted onto four different THY agar plates (Todd–Hewitt broth with 0.5% yeast extract and 1.5% agar). When the fluid was absorbed into the agar, an equal volume of an overlay agar (THY with 0.75% agar and 25 mg liter⁻¹ triphenyl tetrazolium chloride) containing one of the four antibiotics was applied to each THY agar plate. After an overnight incubation at 37 °C, the number of bacterial colonies in the agar plates was enumerated. Opsonization titers were defined as the serum dilution that kills 50% of bacteria.

OPA titer ranking methods

Three different antibody response quantification strategies were developed: rank, strength and extent. Individuals in a cohort were ranked based on vaccine responsiveness across all serotypes using the dense ranking method. For each serotype, participants were assigned a dense rank according to their fold change (after vaccination/before vaccination) in OPA titer levels. Participants with the same fold change levels received the same rank, with the next participants getting the subsequent rank. These individual serotype ranks were then summed to obtain an overall score for each individual. Dense ranking was then applied to these overall scores to determine the final rank for each individual. Individuals with higher fold changes in titer levels across many serotypes ranked higher than others, while those with lower levels across many serotypes received lower ranks. This ranking strategy is robust to outliers (that is, a participant with very high titer levels only for one serotype) and is based on a multivariate approach (using all 13 serotypes) to quantify vaccine responsiveness of individuals. Strength represents the sum of fold change in OPA titer levels across all serotypes and explains the dynamics of baseline and postvaccination changes per sample. Higher scores indicate stronger responses in individuals. An OPA titer of 8 or above was considered a significant response to a specific serotype, forming the basis for the extent strategy^{65,66}. Extent measures the number of serotypes (out of 13) an individual responds to significantly, with higher values indicating a broader response. These measures have unique advantages. To compute the baseline-adjusted fold change for the 13 serotypes, the maxRBA function (titer package in R) with scoreFun set to ‘sum’ was used⁶⁷. The adjusted fold change was then used to rank individuals through a dense ranking approach.

To further evaluate PPSV23 vaccine responses across all 23 serotypes, we reanalyzed OPA titer data from six donors¹¹. These donors received PCV13 first, followed by PPSV23 1 year later. For baseline titers of 13 serotypes that are also in PCV13, we used day 0 measurements before any vaccination, and for the 11 PPSV23-specific serotypes, we used day 360 measurements before PPSV23 vaccination. For postvaccination titer values, we used day 388 measurements. Vaccine response metrics (strength, extent and rank) were computed for all 23 serotypes and the 13-serotype subset. Pearson correlation was used to measure the correlation between vaccine responses from the two sets.

Non-informative donors in our cohorts were identified using baseline (C1) and fold change (C2) thresholds. A baseline cutoff (C1) of 400 and a fold change cutoff (C2) of 8 were used.

Our scoring approach²³ assigned scores of -1 for weak responses (baseline OPA titers of $< C1$ and fold change of $< C2$), 0 for non-informative responses (baseline OPA titers $> C1$) and 1 for strong responses (baseline OPA titer of $< C1$ and fold change of $> C2$) for each serotype. Scores were aggregated across the 13 tested serotypes for each donor. Donors who had seven or more serotypes labeled as non-informative responses were classified as non-informative donors. Others were categorized as strong or weak based on the pre-dominant score.

Determination of CMV seropositivity

Serum samples from 39 participants were assessed for CMV-specific IgG antibodies using an ELISA kit (Aviva Systems Biology). After thawing and centrifugation (6,000g, 1 min), samples and controls were diluted as per the manufacturer's instructions. Results were calculated using nonlinear regression curve fitting based on vendor-supplied controls. Seropositivity was ≥ 1 IU ml⁻¹.

Flow cytometry data generation and analyses

Fluorescence-labeled antibody cocktails for different cell-surface staining panels were premixed in BD Horizon Brilliant Stain Buffer (BD Biosciences) 10 min before staining. Antibody cocktails were added over 100- μ l aliquots of anticoagulated whole blood in a 5-ml FACS tube within 60 min of blood collection. Samples were incubated for 15 min at 25 °C, lysed and fixed with 2 ml of 1 \times FACS lysing solution (BD Biosciences) for 8 min at 25 °C. The lysed samples were washed twice to remove the unbound antibodies, lysed red blood cells and platelets and finally resuspended in 250 μ l of PBS, to which 50 μ l of count bead suspension (Count Bright Absolute Counting Beads, Thermo Fisher) was added for the detection of absolute cell counts. For the analysis of the CD4⁺ T cell compartment, cells were stained with fluorochrome-labeled antibodies targeting the following surface markers: CD3 AF700 (clone UCHT1, BioLegend, 1:200), CD4 APC-Cy7 (clone OKT4, BioLegend, 1:100), CD183 BV421 (clone GO25H7, BioLegend, 1:100), CD196 PE (clone 11A9, BD Biosciences, 1:100), CD185 APC (clone J252D4, BioLegend, 1:100), CD279 FITC (clone MIH4, BD Biosciences, 1:100), CD278 PE-Cy7 (clone C398.4A, BioLegend, 1:200) and CD45RA ECD (clone 3H4, Beckman Coulter, 1:100). Antibody details are provided in Supplementary Table 4a. For analysis of the DC compartment, cells were stained with fluorochrome-labeled antibodies targeting the following surface markers: lineage cocktail (Lin1) FITC (CD3, clone SK7; CD16, clone 3G8; CD19, clone SJ25C1; CD14, clone M Φ P9; CD20, clone L27; CD56, clone NCAM16.2; BD Biosciences, 1:100), HLA-DR APC-eFluor780 (clone LN3, Thermo Fisher, 1:100), CD11c V450 (clone B-ly6, BD Biosciences, 1:100), CD1c PerCP-Cy5.5 (clone L161, BioLegend, 1:100), CD141 APC (clone AD5-14H12, Miltenyi Biotec, 1:100), CD303 PE (clone AC144, Miltenyi Biotec, 1:200), CD86 PE-Cy7 (clone IT2.2, BioLegend, 1:100) and CD40 APC-R700 (clone 5C3, BD Biosciences, 1:50). For analysis of the B cell compartment, cells were stained with fluorochrome-labeled antibodies targeting the following surface markers: CD3 AF700 (clone UCHT1, BD Biosciences, 1:200), CD19 ECD (clone J3-119, Beckman Coulter, 1:100), IgD FITC (clone IA6-2, BD Biosciences, 1:25), CD27 PE (clone M-T271, BD Biosciences, 1:50), CD20 APC (clone 2H7, BioLegend, 1:50), CD86 PE-Cy7 (clone IT2.2, BioLegend, 1:100), CD38 BV421 (clone HIT2, BioLegend, 1:100) and CD138 PE-Cy7 (clone MI15, BD Biosciences, 1:50). The stained cells were acquired with an LSR Fortessa X-20 (BD) and analyzed with FlowJo V9.9.6 software (Treestar). A Wilcoxon matched-pairs signed-rank test assessed differences in cell counts in response to PCV13 or PPSV23 at various time points (days 1, 10, 28 and 60) compared to baseline for high-quality control samples ($n = 35$; 19 men and 16 women). We computed the associations between baseline cellular composition and donor vaccine rank using Pearson correlations.

RNA-seq library generation

Total RNA was isolated from PBMC samples using a Qiagen RNeasy Mini kit (Qiagen) or Arcturus PicoPure (Life Technologies) kits following the manufacturer's protocols. During RNA isolation, DNase treatment was additionally performed using an RNase-free DNase set (Qiagen). RNA quality was checked using an Agilent 2100 Expert Bioanalyzer (Agilent Technologies). RNA quality was reported as a score from 1 to 10, and samples with <8.0 threshold were omitted from the study. RNA-seq libraries were prepared with a KAPA mRNA HyperPrep kit (Roche) according to the manufacturer's instructions. Poly(A) RNA was isolated from 200 ng of total RNA using oligo(dT) magnetic beads and fragmented at 85 °C for 6 min, targeting fragments within the range of

250–300 base pairs. Fragmented RNA was reverse transcribed by incubation for 10 min at 25 °C, followed by incubation for 15 min at 42 °C and inactivation for 15 min at 70 °C. This was followed by second-strand synthesis and A tailing at 16 °C for 30 min and at 62 °C for 10 min. A-tailed, double-stranded cDNA fragments were ligated with Illumina unique adapters (Illumina). Adapter-ligated DNA was purified using AMPure XP beads and amplified by ten cycles of PCR amplification. The final library was cleaned up using AMPure XP beads. Quantification of libraries was performed using real-time quantitative PCR (Thermo Fisher). RNA-seq libraries were sequenced using a NovaSeq (2 \times 150 base pair paired-end reads) to obtain ~100 million reads per sample.

RNA-seq preprocessing

RNA-seq samples were processed using the The Jackson Laboratory's in-house data analysis pipeline. Raw BCL files were converted to fastq files using CASAVA. Trimmomatic (version 0.33) removed adapters, low-quality bases and short reads, and reads were filtered out with more than 50% low-quality bases. The remaining high-quality reads were used for gene expression estimation using the EM algorithm for paired-end read data with default alignment settings. RSEM used bowtie2 as the aligner to align the mapped reads against the hg38 reference genome. Data quality control was performed using Picard (version 1.95) and bamtools to obtain general alignment statistics from the bam file. PREVI2 was excluded due to low-quality issues.

Gene expression data analyses

Gene expression values of PBMC RNA-seq data from 30 samples (15 men and 15 women) were converted into counts per million (CPM) using edgeR (version 3.32.1)⁶⁸. Genes with CPM values less than 0.5 across all samples were filtered out. Differential gene expression analyses were conducted using generalized linear models with default trimmed mean of M values normalization. Significant genes were determined based on *P* values after Benjamini–Hochberg correction for multiple hypothesis testing (FDR *P* value of <0.05 and log₂ (fold change) > ± 0.585). The plasma cell activity score was calculated for each sample by computing the mean expression of genes within the plasma cell (M4.11) gene set¹⁹.

Gene coexpression network analysis

Gene modules associated with vaccine responses were identified using WGCNA (v1.70.3)⁶⁹. A signed coexpression network was constructed using baseline transcriptomes ($n = 30$; 15 men and 15 women) from both cohorts. Gene modules were identified using the blockwiseModules() function in the WGCNA R package (v4.0.4). Pearson correlation served as the correlation metric with a soft threshold of 18, deepSplit was set to 4, and mergeCutHeight was set to 0.25. Sizes of the modules were constrained to 50–2,000 genes. Each module was represented by its first principal component, known as the module eigen gene. Pearson correlations were computed to examine the correlation between modules' eigen genes and metadata, such as PCV13 rank, PPSV23 rank, age, sex and T_H1:T_H17 ratio. Modules with a Pearson correlation of 0.5 and a *P* value of <0.05 were considered significant. For genes present in significant modules (midnight blue and dark green modules), gene set enrichment analysis was conducted using the hypergeometric test from the enrichR package in R⁷⁰. KEGG, Reactome and BioPlanet were used as sources for annotations. Pathways with FDR-corrected *P* values of <0.05 were considered significant using Benjamini–Hochberg for multiple hypothesis test corrections.

Sample processing and blood preparation for scRNA-seq

PBMCs were thawed quickly at 37 °C in DMEM supplemented with 10% fetal bovine serum. After thawing, cells were washed and suspended in PBS containing 0.04% bovine serum albumin. Cell viability was assessed using a Countess II automated cell counter (Thermo Fisher), and up to 12,000 cells (~4,000 cells from each hash-tagged sample) were loaded onto one lane of a 10 \times Genomics Chromium X. Single-cell

capture, barcoding and library preparation were performed using the 10x Chromium platform version 3.1 chemistry following the manufacturer's protocol (CG000388). cDNA and libraries were checked for quality using an Agilent 4200 TapeStation and Thermo Fisher Qubit Fluorometer, quantified by KAPA quantitative PCR and sequenced using 13% of an Illumina NovaSeq 6000 S4 v1.5 200-cycle flow cell lane with a 28-10-10-90 asymmetric read configuration, targeting 6,000 barcoded cells with a minimum sequencing depth of 50,000 read pairs per cell.

Single-cell raw data processing

Illumina base call files for all libraries were converted to FASTQs using bcl2fastq v2.20.0.422 (Illumina) and aligned to the GRCh38 reference assembly with v32 annotations from GENCODE (10x Genomics GRCh38 reference 2020-A) using Cell Ranger multi pipeline v6.1.2 (10x Genomics). The generated gene–cell expression matrix was considered for downstream analysis.

Single-cell gene expression analysis

Count matrices of PBMCs from four men and seven women (six PCV13 SRs and five PCV13 WRs) were obtained. The Scrublet⁷¹ package in Python (v3.8) was used to estimate the doublet score for each sample with an estimated doublet set to 0.6. Cells identified as doublets were removed. The following criteria were used for further cell exclusion: (1) cells with mitochondrial reads greater than 20% and (2) cells with fewer than 500 or more than 4,000 features (Supplementary Table 7). Filtered gene expression matrices were merged and processed using Seurat (v4.1.0). The total number of reads in each individual cell was normalized to CPM using the 'NormalizeData' function. The top 2,000 genes with the highest variance were selected using the 'FindVariableFeatures' function with the 'vst' method. Data were regressed against the percentage of mitochondrial genes and scaled to unit variance using the 'ScaleData' function. Principal-component analysis was performed using the 'RunPCA' function, followed by batch correction across samples using the 'RunHarmony' function from Harmony (v0.1.0). The first 50 principal components were used in the 'FindNeighbors' algorithm to construct the nearest neighbor graph. Next, the Louvain modularity optimization algorithm in the 'FindClusters' function was used to generate the clusters (resolution = 1.2). The 'RunUMAP' function was used to perform UMAP. Multiple rounds of marker identification, semisupervised cell-type annotation using established markers^{72,73}, manual inspection and doublet removal were performed to create the final UMAP. Differentially expressed genes between clusters were identified using the 'FindMarkers' function in Seurat with the Wilcoxon rank-sum test.

Differences in cell frequency between PCV13 SRs and WRs were calculated by computing the frequencies of each immune cell type within PBMCs for each donor. A Wilcoxon rank-sum test was used to evaluate differences in cell proportions between SRs and WRs. Differentially expressed genes between PCV13 SRs and WRs for each cell type were identified from pseudobulked data using the edgeR package in R⁶⁸. Genes with a log₂ (fold change) greater than or less than ±0.25, with an FDR *P* value less than 0.05 and expressed in at least 10% of the cells in both SR and WR groups were considered significantly differentially expressed.

CIBERSORTx analysis

The cellular frequencies of various immune cell subsets in the baseline bulk transcriptomes of PCV13, PPSV23 (from this study) and Fluzone³¹ data were quantified using CIBERSORTx⁷⁴. A signature matrix from the PCV13 scRNA-seq data with cellular annotations was used to deconvolve the bulk transcriptomes (default parameters, permutation = 100).

Fluzone response (GSE45735)

Influenza vaccine responses in healthy young adults (*n* = 5) were assessed using published RNA-seq data⁷⁵. Normalized expression values (reads

assigned per million mapped reads) for the samples at day 0 (baseline) and day 7 after vaccination were obtained from the Gene Expression Omnibus database. The fold difference in expression of constant heavy chain immunoglobulin genes was calculated by subtracting gene expression values at day 7 after vaccination from the baseline values. The mean fold differences in expression of these genes were then compared with those of the respective genes in our data (day 10 baseline).

Fluzone response (GSE59654)

Microarray data (GSE59654)³¹ containing non-frail Fluzone responders (*n* = 5) and non-responders (*n* = 11) were used to assess the association between CD16⁺ NK cell frequency at baseline and Fluzone responsiveness. The data were retrieved, normalized, filtered for probes with a detection *P* value of <0.05 in over 20% of the samples and mapped to genes. Immune deconvolution was performed using CIBERSORTx⁷⁴ with parameters specified in the CIBERSORTx analysis section. CD16⁺ NK cell frequency at baseline was compared between Fluzone responders and non-responders using a Wilcoxon rank-sum test.

Fluad response (GSE211560)

The association between CD16⁺ NK cell frequency at baseline and Fluad responses in older adults³² was assessed by reanalyzing scRNA-seq data from Fluad responders (*n* = 3) and non-responders (*n* = 3) using the Seurat R package (v4.0.4). Baseline samples (responders, *n* = 3; non-responders, *n* = 3) were retrieved and preprocessed with filters described in the original study. Subclusters were annotated based on known markers, and immune cell frequencies in total PBMCs were computed. A Wilcoxon rank-sum test was applied to compare CD16⁺ NK cell frequencies between Fluad responders and non-responders at baseline.

Statistical tests

Statistical analyses for bulk- and scRNA-seq data were performed as described above. *P* values for box plots were calculated using two-sided Wilcoxon rank-sum tests using the `stat_compare_means` function from the `ggpubr` package (v0.4.0). For scatter plots, Pearson's correlation coefficients were reported, and *P* values were calculated using `cor.test` from the `stats` package (v4.0.4) at default settings. The sample size was not determined using a specific statistical test but was based on studies by us¹⁹ and others³². Data distribution was assumed to be normal, but this was not formally tested.

Reporting summary

Further information on research design is available in the Nature Portfolio Reporting Summary linked to this article.

Data availability

Raw files of the bulk- and scRNA-seq data generated in this study are available in dbGAP under the accession code [phs002361.v2.p1](https://dbgap.ncbi.nlm.nih.gov/ah/nsl/study.cgi?study_id=phs002361.v2.p1). The processed bulk and single-cell transcriptome data have been deposited in NCBI Gene Expression Omnibus under the accession numbers [GSE247276](https://www.ncbi.nlm.nih.gov/geo/query/acc.cgi?acc=GSE247276) and [GSE247277](https://www.ncbi.nlm.nih.gov/geo/query/acc.cgi?acc=GSE247277). Source data are provided with this paper.

Code availability

All the custom code used to analyze the data has been deposited in GitHub and can be accessed using the following link: https://github.com/sathyabaarathir/pneumococcal_vaccine_BIS.

References

- Cooper, D. et al. The 13-valent pneumococcal conjugate vaccine (PCV13) elicits cross-functional opsonophagocytic killing responses in humans to *Streptococcus pneumoniae* serotypes 6C and 7A. *Vaccine* **29**, 7207–7211 (2011).
- Jódar, L. et al. Serological criteria for evaluation and licensure of new pneumococcal conjugate vaccine formulations for use in infants. *Vaccine* **21**, 3265–3272 (2003).

67. Avey, S. et al. Seasonal variability and shared molecular signatures of inactivated influenza vaccination in young and older adults. *J. Immunol.* **204**, 1661–1673 (2020).
68. Robinson, M. D., McCarthy, D. J. & Smyth, G. K. edgeR: a Bioconductor package for differential expression analysis of digital gene expression data. *Bioinformatics* **26**, 139–140 (2010).
69. Langfelder, P. & Horvath, S. WGCNA: an R package for weighted correlation network analysis. *BMC Bioinformatics* **9**, 559 (2008).
70. Xie, Z. et al. Gene set knowledge discovery with Enrichr. *Curr. Protoc.* **1**, e90 (2021).
71. Wolock, S. L., Lopez, R. & Klein, A. M. Scrublet: computational identification of cell doublets in single-cell transcriptomic data. *Cell Syst.* **8**, 281–291 (2019).
72. Mace, E. M. Human natural killer cells: form, function, and development. *J. Allergy Clin. Immunol.* **151**, 371–385 (2023).
73. Mace, E. M. & Orange, J. S. Emerging insights into human health and NK cell biology from the study of NK cell deficiencies. *Immunol. Rev.* **287**, 202–225 (2019).
74. Newman, A. M. et al. Determining cell type abundance and expression from bulk tissues with digital cytometry. *Nat. Biotechnol.* **37**, 773–782 (2019).
75. Henn, A. D. et al. High-resolution temporal response patterns to influenza vaccine reveal a distinct human plasma cell gene signature. *Sci. Rep.* **3**, 2327 (2013).

Acknowledgements

We thank T. Helenius for aid in scientific writing, M. Collet for help with dbGAP data upload, research staff in the UConn Center on Aging for their help in recruitment and sample collection and D. Luo and P. Gabriel from the JAX Genomic Technologies and Single Cell cores for help with generating the sequencing data. The JAX single-cell service is supported, in part, by the JAX Cancer Center P30 CA034196 (to K.P., D.U., J.B., D.C. and S.P.). We thank members of the Ucar lab for critical feedback during the progress of the study. This study was made possible by generous financial support from NIH grants under award numbers R01AG052608 (to J.B.), U01AI165452 (to D.U. and G.A.K.), P30AG067988 Older Americans Independence Pepper Center (to G.A.K.) and R01AI142086 (to D.U. and J.B.) and JAX Cancer Center Brooks Scholarship (to S.R.). Opinions, interpretations, conclusions and recommendations are solely the responsibility of the authors and do not necessarily represent the official views of the NIH.

Author contributions

J.B. designed the study and raised the funds. J.B., G.A.K. and D.U. cosupervised the study. G.A.K. co-ordinated human studies and sample collection. L.K.-P. developed recruitment strategies and facilitated blood collection. M.H.N. co-ordinated and generated OPA titer data. R.M. and R.R. generated flow cytometry, RNA-seq and CMV data. S.R., F.E.-D. and O.E.K. analyzed the data. D.U., F.E.-D., J.B. and S.R. wrote the paper. V.P., K.P., S.P., D.C., D.N.-B. and D.C.L. helped with data interpretation and edited the paper. All authors revised the paper and figures before submission.

Competing interests

While this study was performed, J.B. served on the Board of Directors for Neovacs, is a Board of Directors member and stockholder for Ascend Biopharmaceuticals, Scientific Advisory Board member for Cue Biopharma and stockholder for Sanofi. M.H.N. is an employee of the University of Alabama at Birmingham, which has intellectual property on the target bacteria used for the opsonophagocytosis assays. S.P. serves on the Scientific Advisory Board for Shoreline Biosciences and Qihan Biotechnology and is a Scientific Consultant for Qihan Biotechnology and the Genomics Institute of the Novartis Research Foundation. The other authors declare no competing interests.

Additional information

Extended data is available for this paper at <https://doi.org/10.1038/s41590-023-01717-5>.

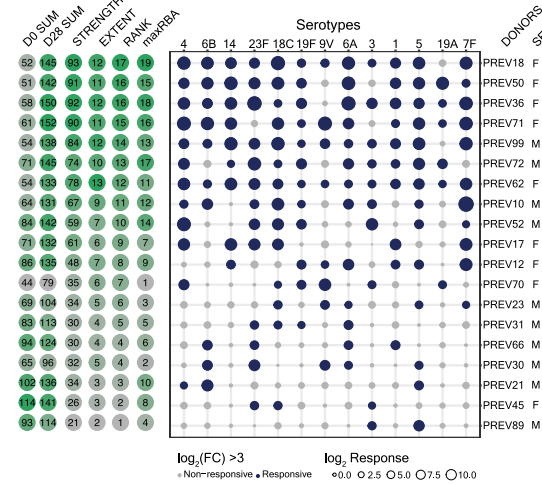
Supplementary information The online version contains supplementary material available at <https://doi.org/10.1038/s41590-023-01717-5>.

Correspondence and requests for materials should be addressed to Duygu Ucar.

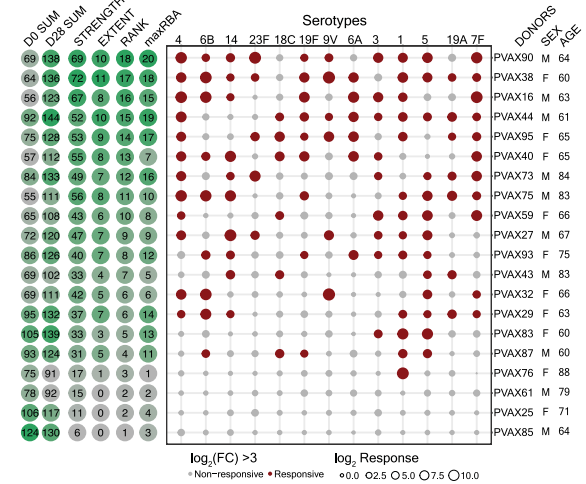
Peer review information *Nature Immunology* thanks Jeremy Brown, Stephen Gordon and the other, anonymous, reviewer(s) for their contribution to the peer review of this work. Primary Handling Editor: L. A. Dempsey, in collaboration with the *Nature Immunology* team.

Reprints and permissions information is available at www.nature.com/reprints.

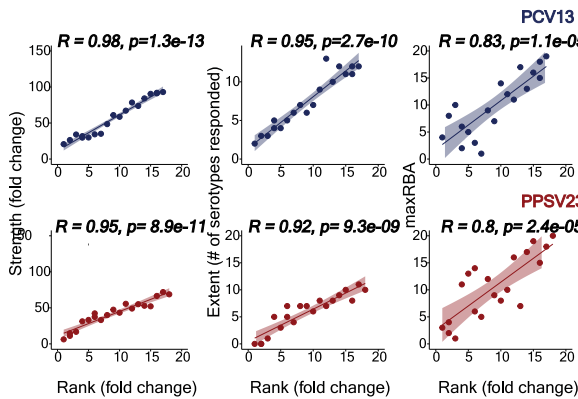
a Responses to Prevnar (PCV13)



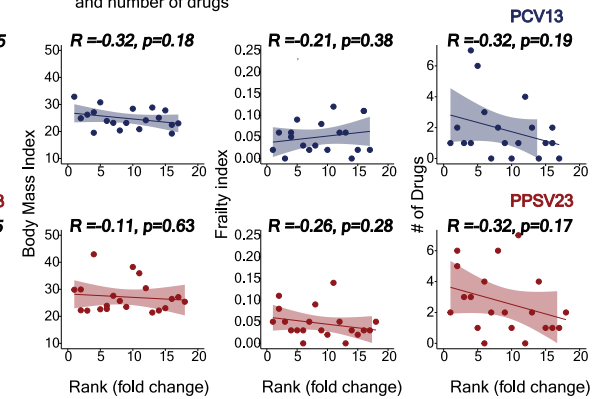
b Responses to Pneumovax (PPSV23)



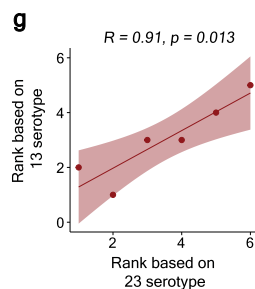
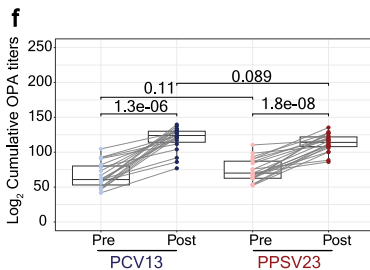
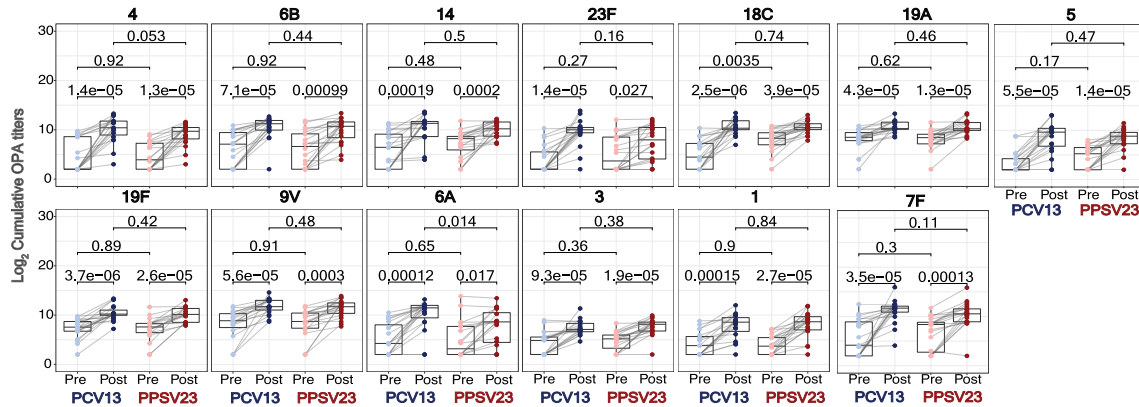
c Correlation between rank and strength, extent and maxRBA



d Correlation between rank and body mass index, frailty index and number of drugs



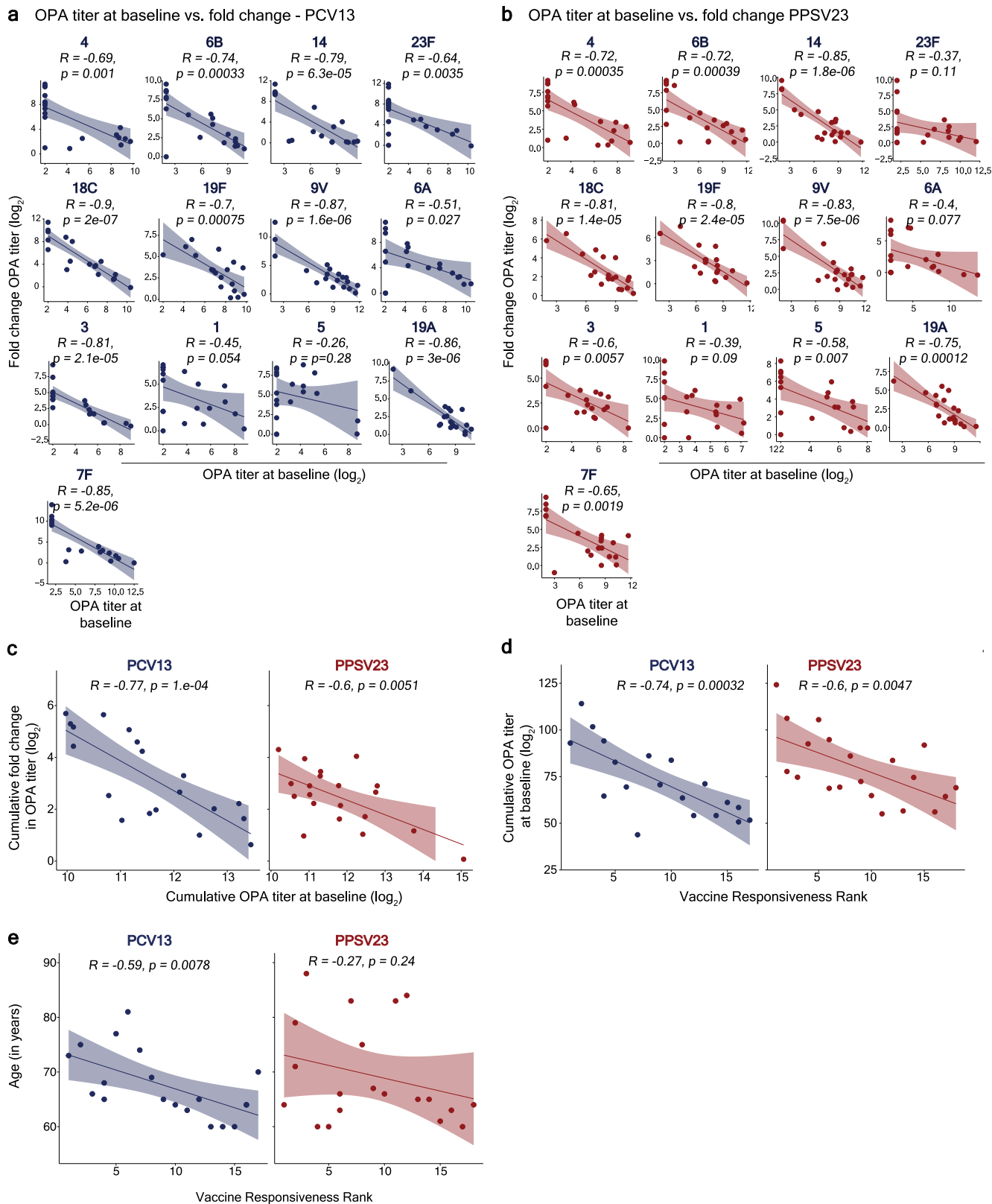
e Antibody responses per serotype



Extended Data Fig. 1 | See next page for caption.

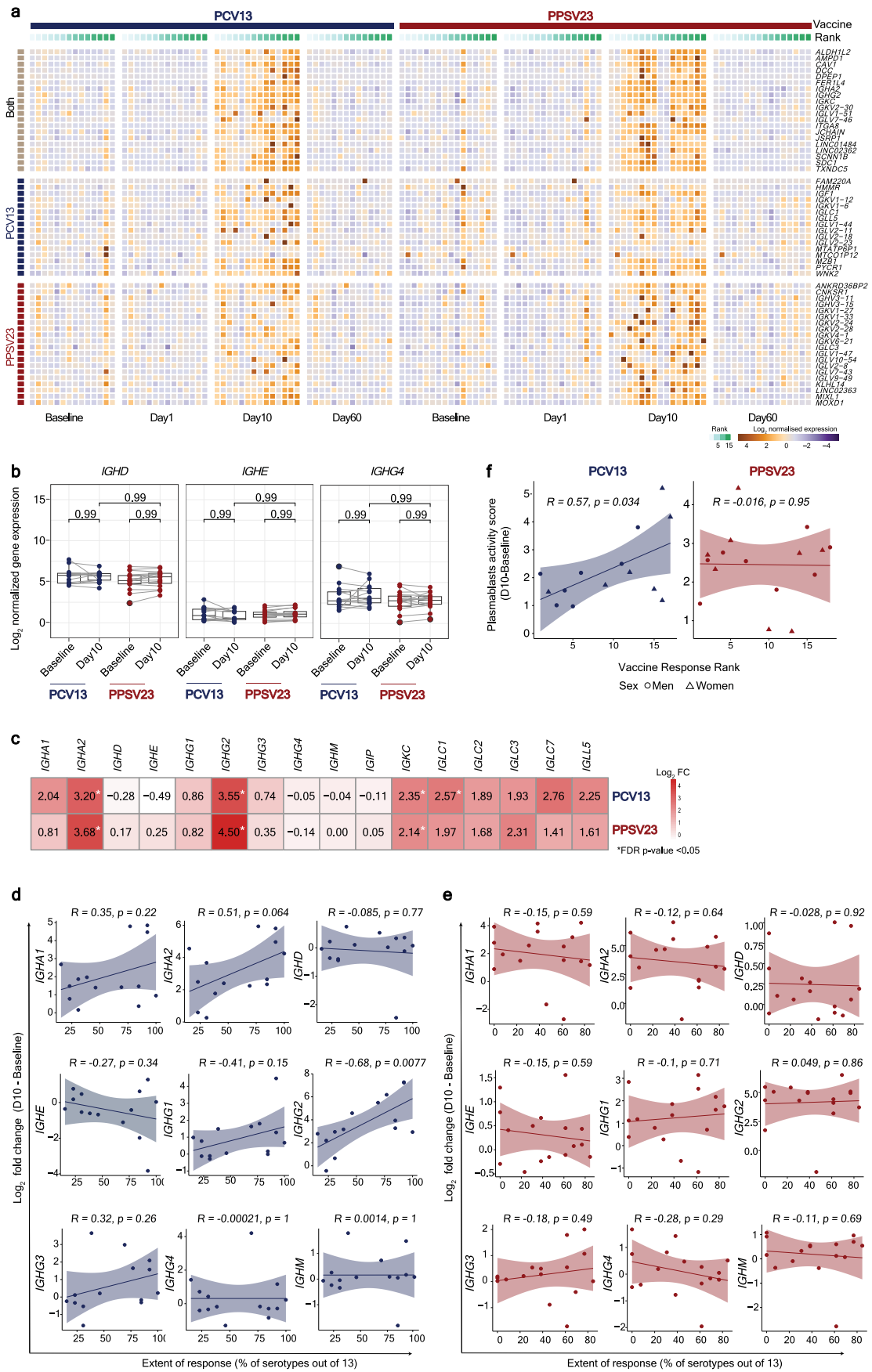
Extended Data Fig. 1 | Functional antibody response to PCV13 and PPSV23. Bubble plot showing the fold change in the antibody titers for individual serotypes in response to PCV13 (n = 19) **a**) and PPSV23 (n = 20) **b**). The size of the dots represents the magnitude of the fold change (FC) value, and the color indicates significant response ($\text{Log}_2 \text{FC}$ is > 3): blue for PCV13 and red for PPSV23. Donors are ordered from top to bottom according to the vaccine response Rank. On the left side, D0 SUM (sum of pre-vaccination OPA titers to 13 serotypes), D35 SUM (sum of 28 days post-vaccination OPA titers to 13 serotypes), the Strength, the Extent, the Rank and the maxRBA rank (sum of baseline adjusted fold changes to 13 serotypes) for each donor is displayed. **c**) Correlation between the Rank and the Strength, the Extent, the maxRBA for PCV13 (n = 19; top panel) and PPSV23 (n = 20; bottom panel). **d**) Correlation between the Rank and body

mass index (BMI), frailty index (FI) and number of concomitant drugs. **e**) OPA titers (Log_2) for individual serotypes showing the connecting lines between Pre and post-vaccination. **f**) Pre-vaccination and post-vaccination cumulative OPA titers (expressed as sum Log_2) excluding serotype 6A. **g**) Correlation of Rank determined from all 23 serotypes and a subset of 13 serotypes present in the PCV13 in an independent cohort. The Pearson correlation metric was used to perform correlation analysis (c, d, and g) and p-value was generated using two-sided t-test. Boxplots display the median and IQR (25–75%), with whiskers representing the upper- and lower-quartile $\pm 1.5 \times \text{IQR}$. The Wilcoxon matched-pairs signed-rank test (two-sided) was used in to compare the difference in mean between pre- and post-vaccination OPA titers for 13 serotypes (e, f) in PCV13 and PPSV23. The 'n' represents number of biological replicates.



Extended Data Fig. 2 | Baseline OPA titers inversely correlate with fold change in OPA titers and vaccine responsiveness ranks. Correlation between baseline OPA titers and their post-vaccination fold change for individual serotypes for PCV13 (n = 19) **a**) and PPSV23 (n = 20) **b**). **c**) Association between cumulative baseline OPA titer and fold change for both PCV13 (n = 19) and PPSV23 (n = 20). Both baseline and fold change in OPA titers are expressed on a \log_2

scale (a, b, c). **d**) Correlation between cumulative baseline OPA titer and vaccine responsiveness rank for both vaccines. **e**) Correlation between Rank and age (in years) for PCV13 and PPSV23. The Pearson correlation metric was used to perform correlation analysis and p-value was generated using two-sided t-test. The 'n' represents number of biological replicates.



Extended Data Fig. 3 | See next page for caption.

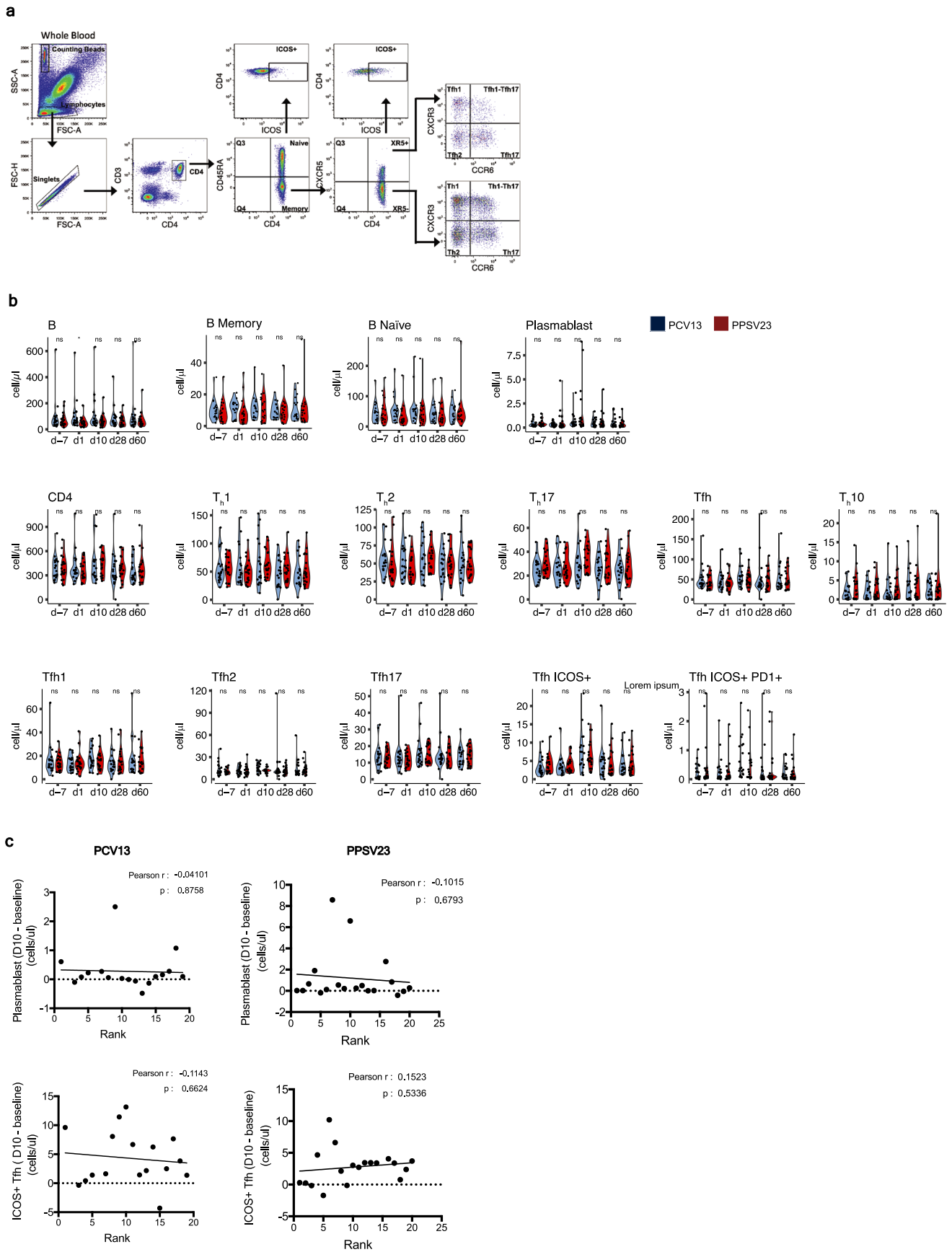
Extended Data Fig. 3 | Differential transcriptional changes in response to

PCV13 and PPSV23 at day 10. a) Heatmap showing differentially expressed genes between Day 10 and baseline, using the normalized gene expression. Differentially expressed genes that are common for both vaccines or show differential expression only in PCV13 or PPSV23 are grouped separately.

b) Boxplots of the normalized expression of genes coding for the constant region of immunoglobulin heavy chain structure. **c)** Heatmap of differential expressed genes coding for the constant region of immunoglobulin heavy chain structure at Day 10 in response to PCV13 and PPSV23. Genes with a FC >1.5-fold difference and a FDR p-value <0.05 are marked with stars. **d)** Correlation analysis between the

fold difference in immunoglobulin genes (gene expression at Day 10 - baseline) and the extent of the response (% of serotypes out of 13) for PCV13.

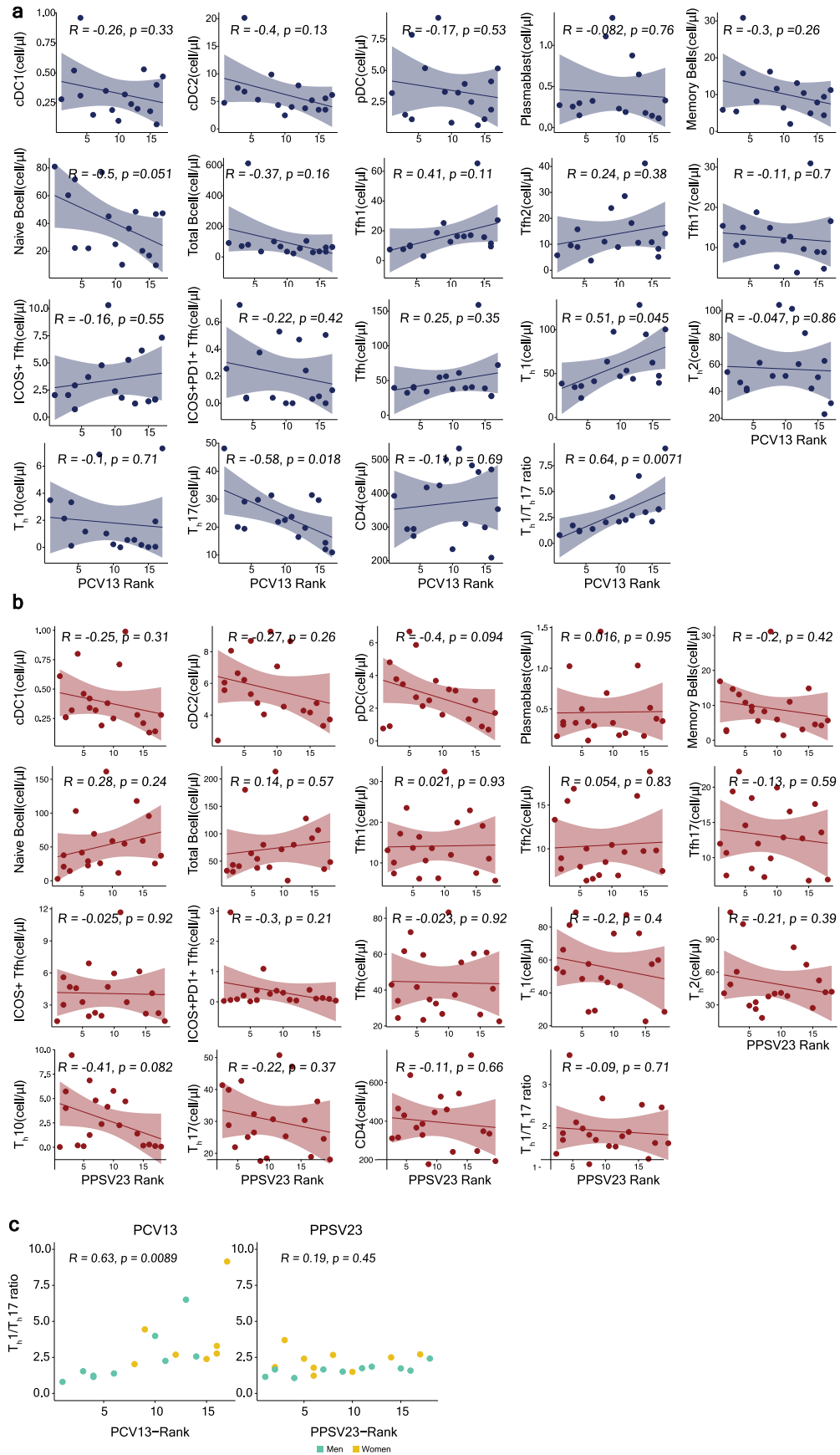
e) Correlation analysis between the fold difference in immunoglobulin genes (gene expression at Day 10 - baseline) and the extent of the response (% of serotypes out of 13) for PPSV23. **f)** Correlation between the plasmablasts activity scores (Day 10 vs. baseline) and vaccine responsiveness Rank. The Pearson correlation metric was used to perform correlation analysis (a, c, and d). The Wilcoxon matched-pairs signed-rank test (two-sided) was used to compare the expression of immunoglobulin genes at baseline and Day 10 for PCV13 and PPSV23 (c). The 'n' represents number of biological replicates.



Extended Data Fig. 4 | See next page for caption.

Extended Data Fig. 4 | No association between changes in plasmablasts and ICOS⁺ Tfh cells at Day 10 and responses to both vaccines. **a)** Representative plots showing the gating strategy for the characterization by flow cytometry of the different memory CD4⁺ T cell populations. **b)** Comparative analysis of the absolute number of the different cell types between PCV13 (n = 16) and PPSV23 (n = 19) cohorts over time. **c)** Correlation between fold difference in plasmablasts cell numbers (d10 - baseline) and vaccine responsiveness Rank (top panel).

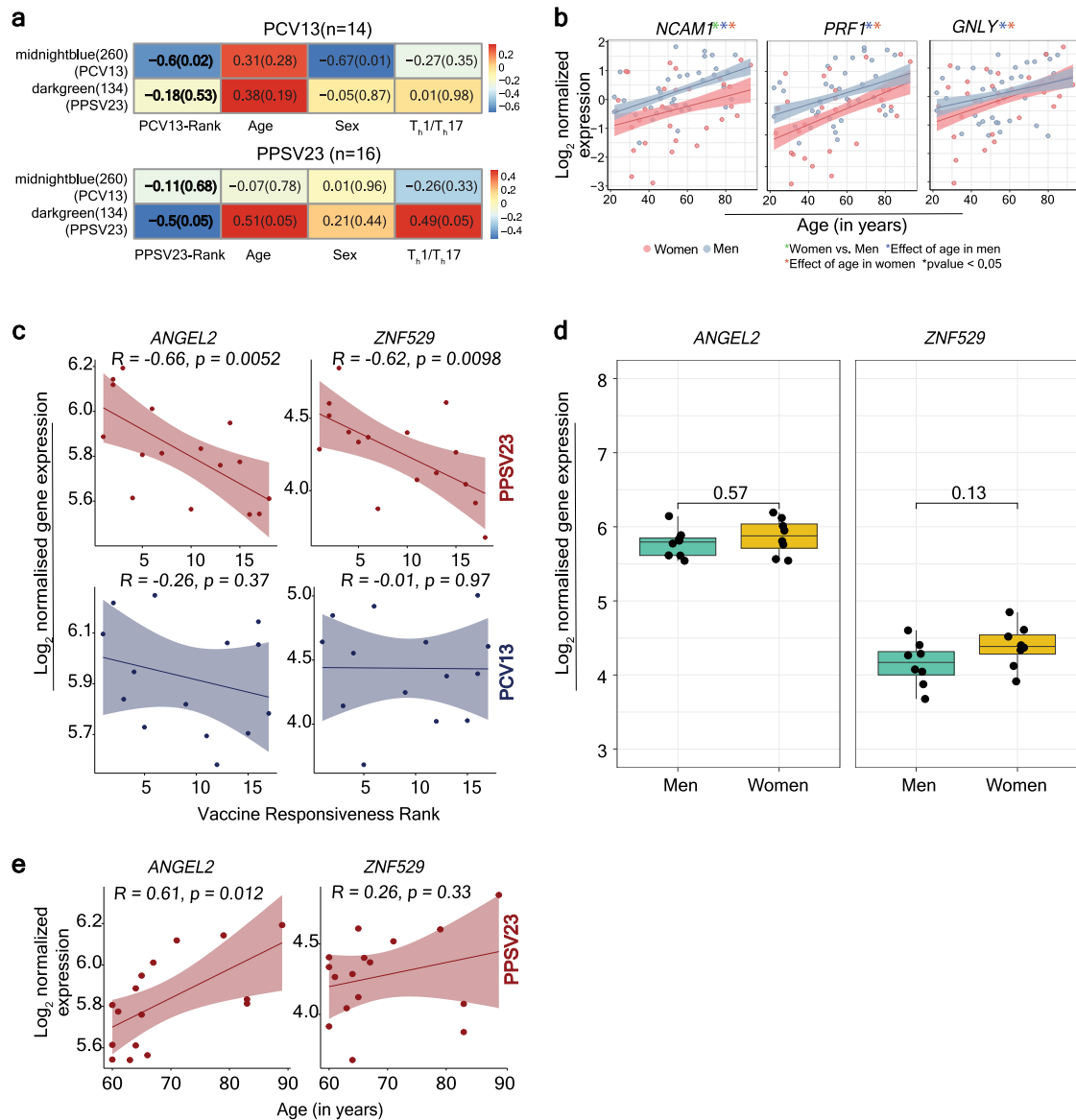
Correlation between fold difference in ICOS⁺ Tfh cell numbers (d10 - baseline) and vaccine responsiveness Rank (bottom panel). The Wilcoxon Rank sum test was used to compare the absolute numbers of different cell types: * (p < 0.05), ** (p < 0.01), *** (p < 0.001), **** (p < 0.0001) (b). The Pearson correlation metric was used to perform correlation analysis (a, b, and c), and the p-value was computed using two-sided t test (c). The 'n' represents number of biological replicates.



Extended Data Fig. 5 | See next page for caption.

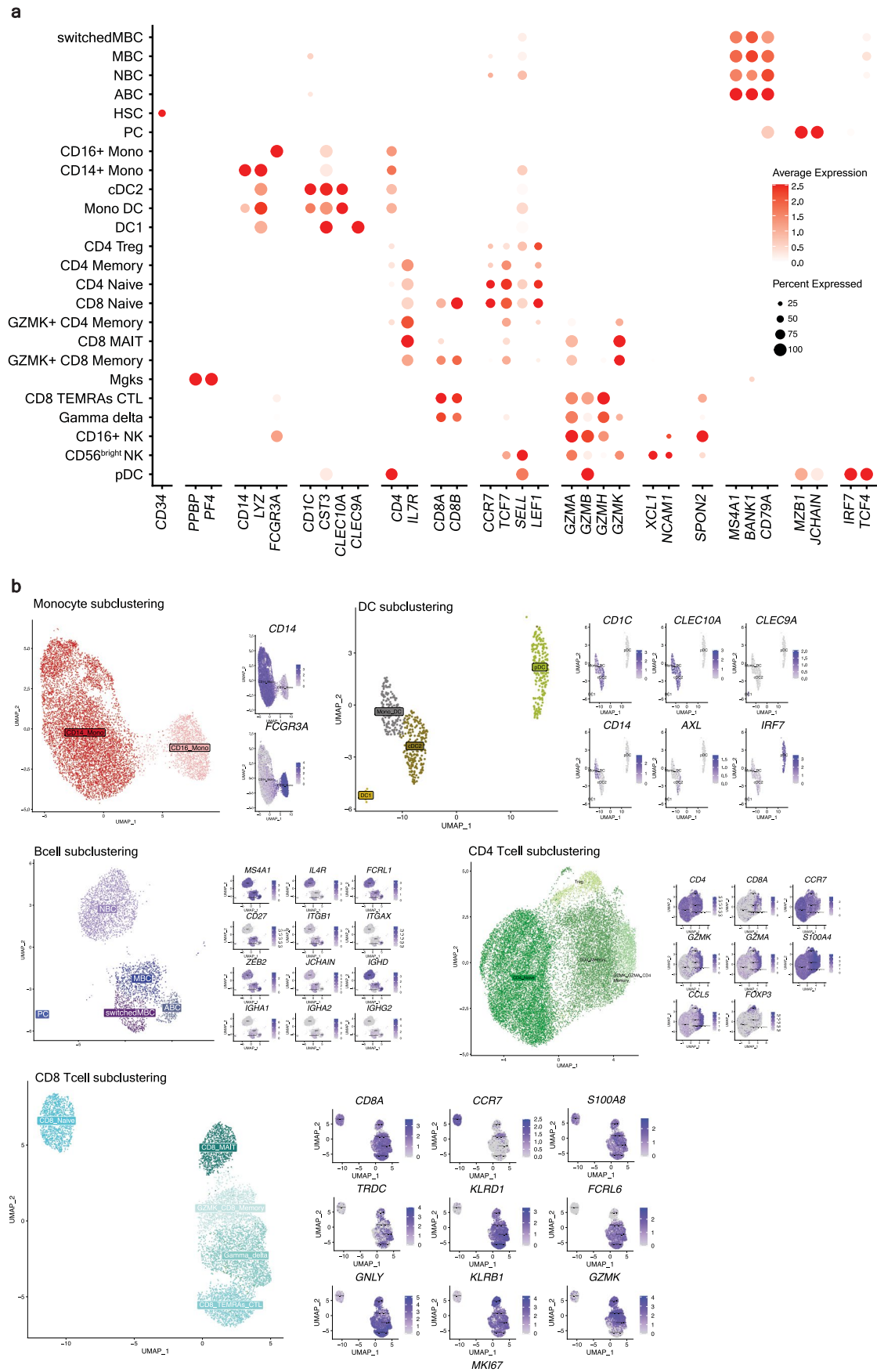
Extended Data Fig. 5 | Higher T_H1/T_H17 ratio mount stronger responses to PCV13. **a)** Correlation analysis between PCV13 Rank and the absolute numbers (cells/ul) of the different cell populations at baseline (d-7) (n = 16). **b)** Correlation analysis between PPSV23 Rank and the absolute numbers (cells/ul) of the different cell populations at baseline (d-7) (n = 19). **c)** Correlation analysis of

T_H1/T_H17 ratio and vaccine responsiveness Ranks of PCV13 (n = 16) and PPSV23 (n = 19), respectively. The Pearson correlation metric was used to perform correlation analysis (a, b, and c), and the p-value was computed using two-sided t test. The 'n' represents number of biological replicates.

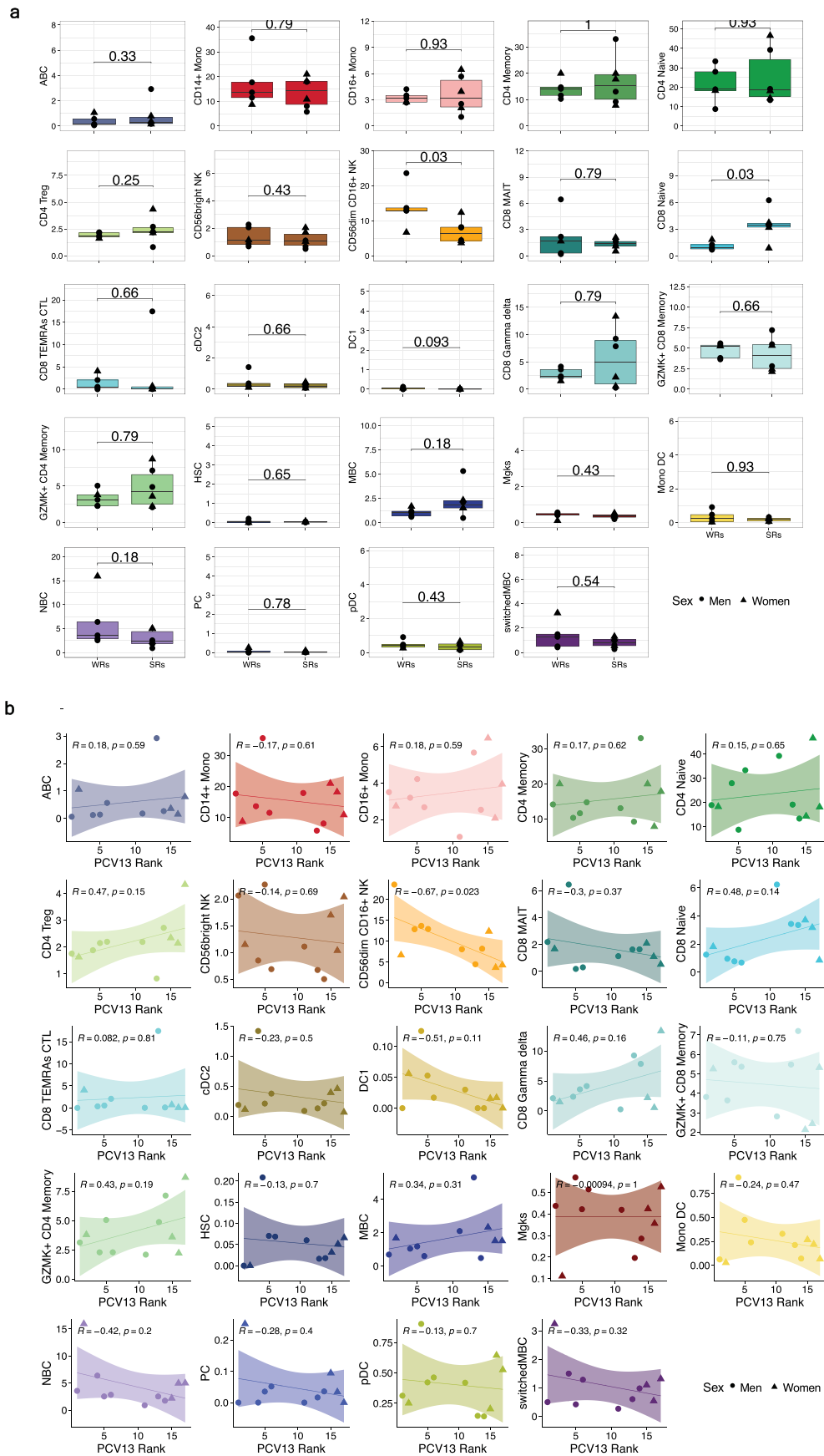


Extended Data Fig. 6 | Baseline expression of ‘darkgreen module’ genes negatively associated with PPSV23 responses. **a**) Heatmap showing the modules correlated with PCV13 Rank, PPSV23 Rank, sex, age and T_n1/T_n17 ratio. **b**) Correlation between the expression of cytotoxic genes and age (in years) in an independent dataset. **c**) Correlation analysis between top correlates of darkgreen module (*ANGEL2*, and *ZNF529*) and PPSV23 Rank (n = 16). Correlation analysis between top correlates of darkgreen module (*ANGEL2*, and *ZNF529*) and PCV13 Rank (n = 14). **d**) Boxplot showing the expression of top correlates of

darkgreen module (*ANGEL2*, and *ZNF529*) in men and women (n = 16). **e**) Association between *ANGEL2*, and *ZNF529* expression with age (in years). Boxplots display the median and IQR (25–75%), with whiskers representing the upper- and lower-quartile $\pm 1.5 \times$ IQR. The Wilcoxon Rank sum test (two-sided) was used to compare the expression of genes in men and women (e). Correlation analysis was performed using the Pearson correlation metric (b,c,e), and the p-value was computed using two-sided t test. The ‘n’ represents number of biological replicates.



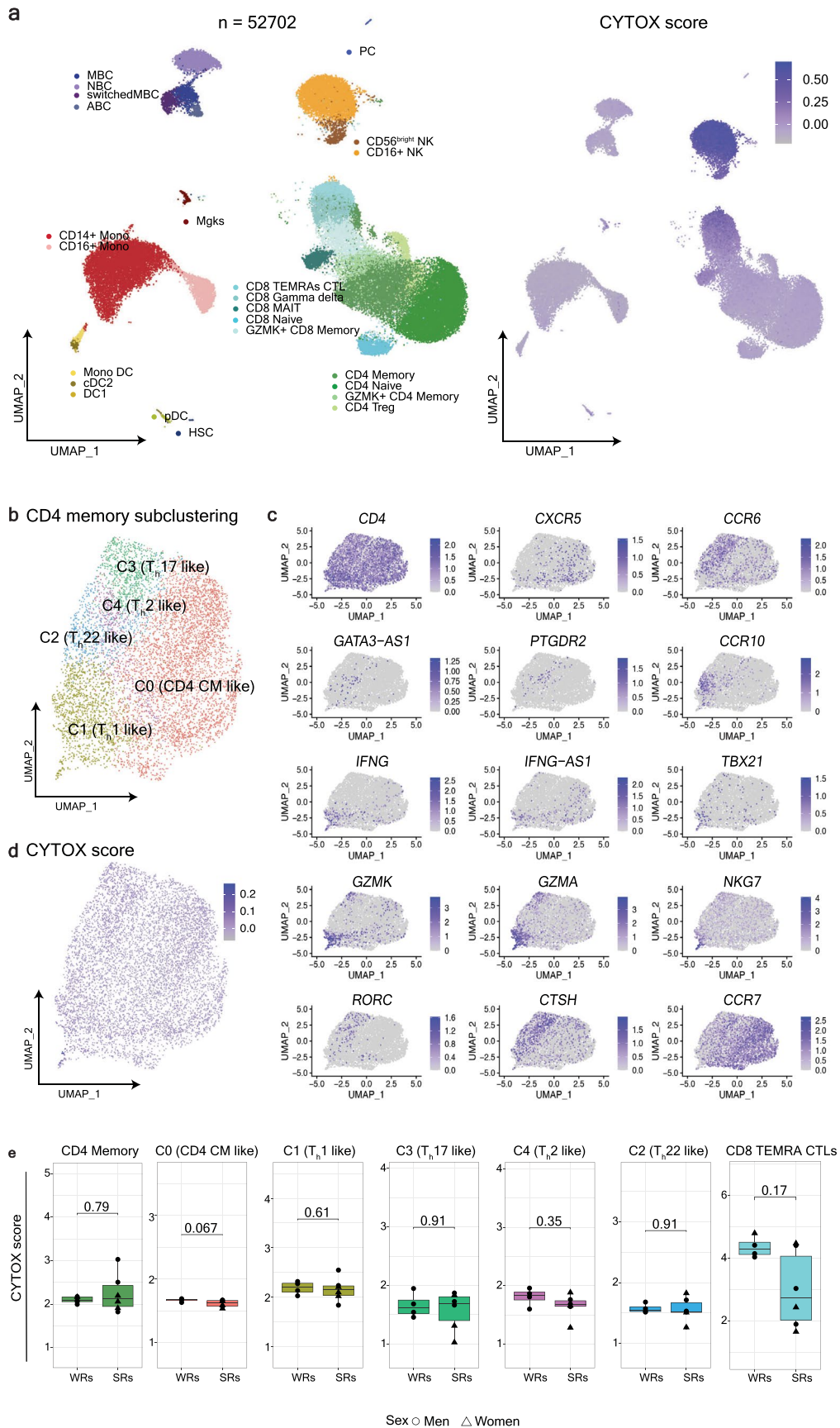
Extended Data Fig. 7 | Subclustering of baseline PBMC RNA-Seq at the single-cell level. a) Dot plot showing the marker gene expression for each subset detected in the PBMC scRNA-seq data. **b)** Single cell subclustering of Monocytes, DCs, B, CD4 and CD8 T cells. Feature plots showing the known markers in blue.



Extended Data Fig. 8 | See next page for caption.

Extended Data Fig. 8 | Differential immune cell frequencies between PCV13 SRs and WRs. a) Stacked bar plot showing immune cell compositions in strong responders (SRs, n = 6) and weak responders (WRs, n = 5). Cell types showing significant difference between SRs and WRs are marked with a star (pvalue < 0.05 starred in red). **b)** Boxplot showing the frequency of different immune cell subsets in SRs and WRs. **c)** Correlation analysis between PCV13 rank and the frequency

of different immune cell subsets. Boxplots display the median and IQR (25–75%), with whiskers representing the upper- and lower-quartile $\pm 1.5 \times$ IQR. The Wilcoxon Rank sum test (two-sided) was used to compare the cell percentages between PCV13- SRs and WRs. Correlation analysis was performed using the Pearson correlation metric and p-value was computed using two-tailed t-test. The 'n' represents number of biological replicates.

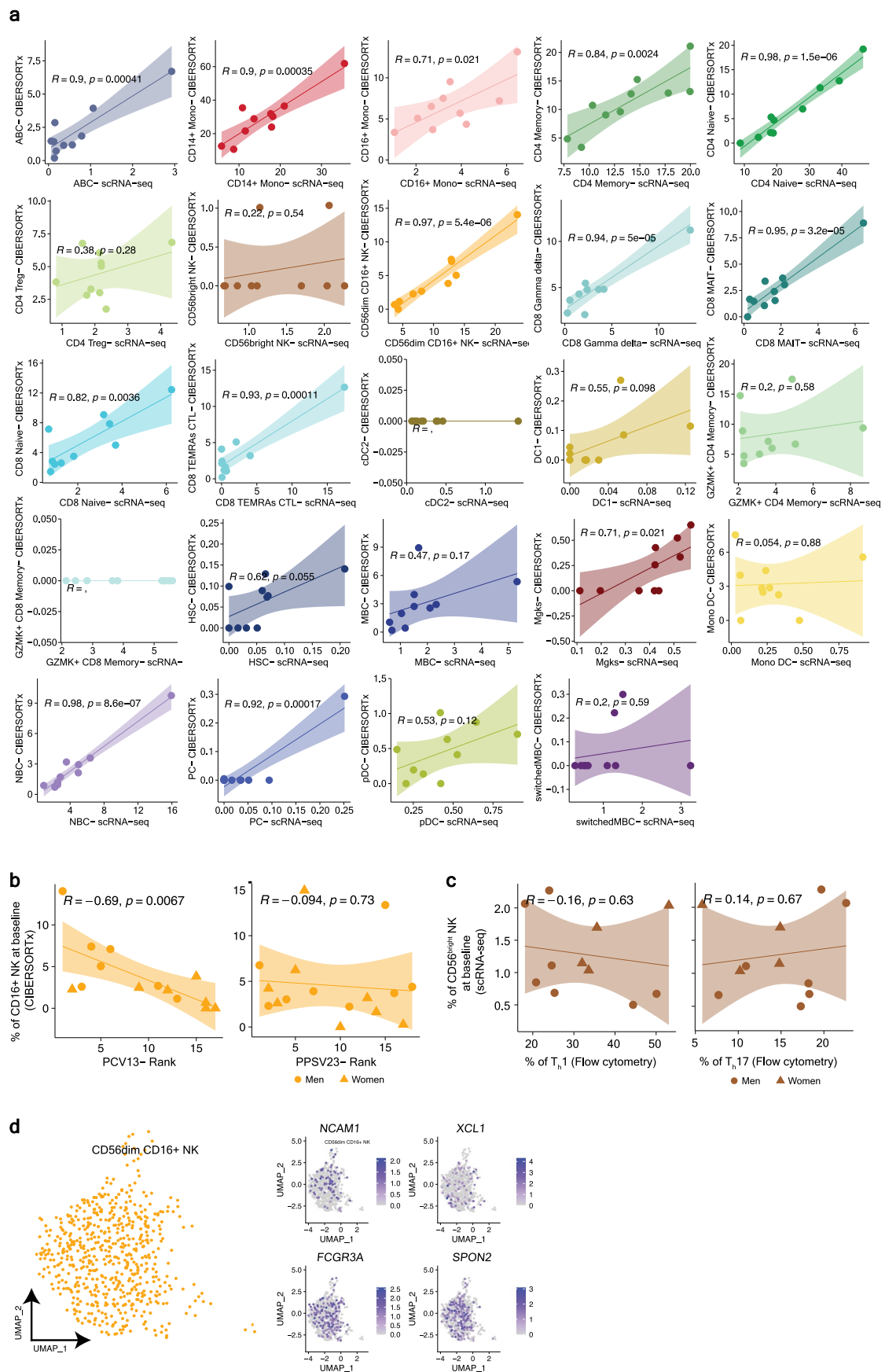


Extended Data Fig. 9 | See next page for caption.

Extended Data Fig. 9 | The CYTOX Signature stems from CD16+ NK Cells.

a) UMAP representation of PBMCs derived from 11 PCV13 donors, consisting of 6 strong responders (SRs) and 5 weak responders (WRs). This visualization encompasses 24 clusters from a total of 52,702 cells, each color-coded by their respective immune cell type. An accompanying feature plot elucidates the distribution of the CYTOX score across these 24 distinct immune cell populations. The CYTOX score is derived from the expression of genes from module associated with PCV13 response (midnightblue module), showing a Pearson correlation coefficient greater than 0.5. **b)** Subclustering of CD4⁺ memory cells highlight subsets expressing marker genes for C0 (central memory

like cells), C1 (T_h1 like), C2 (T_h22 like), C3 (T_h17 like) and C4 (T_h2 like). **c)** A feature plot to show marker gene expression for memory CD4⁺ subsets. **d)** A feature plot showing CYTOX score for memory CD4⁺ T cells. **e)** Comparison of CYTOX scores for 6 SRs and 5 WRs for each memory CD4⁺ subset and CD8⁺ TEMRA CTLs. Boxplots display the median and IQR (25–75%), with whiskers representing the upper- and lower-quartile $\pm 1.5 \times$ IQR. The Wilcoxon Rank sum test (two-sided) was employed to assess differences in the CYTOX scores between the PCV13 SRs and WRs across these CD4 memory subsets and CD8⁺ TEMRA CTLs. The 'n' represents number of biological replicates.



Extended Data Fig. 10 | See next page for caption.

Extended Data Fig. 10 | Association between baseline CD16⁺ NK frequency estimated from CIBERSORTx and PCV13 vaccine responses. **a)** Correlation between pre-vaccination cell frequency estimated by scRNA-seq and CIBERSORTx for different immune subtypes. **b)** Correlation analysis of CD16⁺ NK frequency at baseline and vaccine responsiveness Ranks of PCV13 (n = 14) and PPSV23 (n = 16), respectively. For the correlation analysis with PPSV23-Rank, cell frequency estimated by CIBERSORTx from the bulk PPSV23 baseline transcriptomes (n = 16) was considered. **c)** Correlation analysis of CD56^{bright} NK

frequency (n = 11) and T_H1, and T_H17 frequency at baseline. Pearson correlation was used to perform correlation analysis (a,b,c) and p-value was computed using two-tailed t-test. **d)** UMAP representation of CD16⁺ NK subsets in flud responders (n = 3) and non-responders (n = 3) at baseline. Feature plots showing *NCAMI*, *XCL1*, *FCG3RA* and *SPON2* in CD16⁺ NK cells in blue. Correlation analysis was performed using the Pearson correlation metric and p-value was computed using two-tailed t-test. The 'n' represents number of biological replicates.

Reporting Summary

Nature Portfolio wishes to improve the reproducibility of the work that we publish. This form provides structure for consistency and transparency in reporting. For further information on Nature Portfolio policies, see our [Editorial Policies](#) and the [Editorial Policy Checklist](#).

Statistics

For all statistical analyses, confirm that the following items are present in the figure legend, table legend, main text, or Methods section.

n/a | Confirmed

- The exact sample size (n) for each experimental group/condition, given as a discrete number and unit of measurement
- A statement on whether measurements were taken from distinct samples or whether the same sample was measured repeatedly
- The statistical test(s) used AND whether they are one- or two-sided
Only common tests should be described solely by name; describe more complex techniques in the Methods section.
- A description of all covariates tested
- A description of any assumptions or corrections, such as tests of normality and adjustment for multiple comparisons
- A full description of the statistical parameters including central tendency (e.g. means) or other basic estimates (e.g. regression coefficient) AND variation (e.g. standard deviation) or associated estimates of uncertainty (e.g. confidence intervals)
- For null hypothesis testing, the test statistic (e.g. F , t , r) with confidence intervals, effect sizes, degrees of freedom and P value noted
Give P values as exact values whenever suitable.
- For Bayesian analysis, information on the choice of priors and Markov chain Monte Carlo settings
- For hierarchical and complex designs, identification of the appropriate level for tests and full reporting of outcomes
- Estimates of effect sizes (e.g. Cohen's d , Pearson's r), indicating how they were calculated

Our web collection on [statistics for biologists](#) contains articles on many of the points above.

Software and code

Policy information about [availability of computer code](#)

Data collection	Flow cytometry data was generated using BD LSR Fortessa X-20. Bulk RNA Sequencing data was generated using Illumina NovaSeq (2x150 bp paired end reads) platform. Single cell RNA sequencing was generated using the 10x Chromium platform version 3.1 chemistry platform.
Data analysis	FlowJo V9.9.6 software (Treestar Inc); Trimmomatic (v0.33); Picard (v1.95); Cell Ranger multi pipeline v6.1.2; CIBERSORTx; RStudio v3.28.1; Python 3.8; Scrublet (v3.8); WGCNA (v1.70.3); edgeR (version 3.32.1); Seurat (v4.1.0); ggpubr (v0.4.0); Harmony (v0.1.0). The scripts used for the data processing and analysis are available here : https://github.com/sathyabaarathisr/pneumococcal_vaccine_BIS/

For manuscripts utilizing custom algorithms or software that are central to the research but not yet described in published literature, software must be made available to editors and reviewers. We strongly encourage code deposition in a community repository (e.g. GitHub). See the Nature Portfolio [guidelines for submitting code & software](#) for further information.

Data

Policy information about [availability of data](#)

All manuscripts must include a [data availability statement](#). This statement should provide the following information, where applicable:

- Accession codes, unique identifiers, or web links for publicly available datasets
- A description of any restrictions on data availability
- For clinical datasets or third party data, please ensure that the statement adheres to our [policy](#)

Raw files of the bulk and single cell RNAseq data generated in this study is available in the dbGAP under the accession code phs002361.v2.p1. The processed bulk and single-cell transcriptome data has been deposited in NCBI GEO under the accession numbers GSE247276 and GSE247277. GEO IDs of previously published datasets used in this study: GSE45735, GSE59654 and GSE211560.

Research involving human participants, their data, or biological material

Policy information about studies with [human participants or human data](#). See also policy information about [sex, gender \(identity/presentation\), and sexual orientation](#) and [race, ethnicity and racism](#).

Reporting on sex and gender	We studied sex differences in our data and report the differences observed between sexes.
Reporting on race, ethnicity, or other socially relevant groupings	Race and ethnicity information is provided in Supplementary Table S1.
Population characteristics	The population characteristics and demographics are provided in Supplementary Table s1.
Recruitment	All the participants in the study were recruited by the UConn Center on Aging Recruitment and Community Outreach Research Core (http://health.uconn.edu/aging/research/research-cores/). There was no self-selection conflict involved.
Ethics oversight	Study was conducted following approval by the UConn Health Center Institutional Review Board (IRB Number: 16-071J-1) and registration on ClinicalTrials.gov (NCT03104075). All participants provided informed consent and were compensated for their time and study visits.

Note that full information on the approval of the study protocol must also be provided in the manuscript.

Field-specific reporting

Please select the one below that is the best fit for your research. If you are not sure, read the appropriate sections before making your selection.

- Life sciences Behavioural & social sciences Ecological, evolutionary & environmental sciences

For a reference copy of the document with all sections, see nature.com/documents/nr-reporting-summary-flat.pdf

Life sciences study design

All studies must disclose on these points even when the disclosure is negative.

Sample size	<p>PCV13 cohort: 10 men and 9 women. PPSV23 cohort: 10 men and 10 women. OPA assay was performed for all 39 participants (20 men and 19 women) at baseline and day 28 post vaccination. Flow cytometric analysis was performed for 35 participants (19 men and 16 women) at baseline, day 1, day 10, day 28 and day 60. Bulk RNAseq was performed for 14 (7 men and 7 women) participants from the PCV13 cohort and 16 (8 men and 8 women) participants from the PPSV23 cohort at four different timepoints (baseline, day 1, day 10, day 28). scRNAseq was performed for 4 men and 7 women from PCV13 cohort at baseline. No statistical test was used to determine the number of samples. However, the sample size used was determined as appropriate to detect the effect of vaccine response based on our previous studies and those conducted by others.</p> <p>Riese, P. et al. Distinct immunological and molecular signatures underpinning influenza vaccine responsiveness in the elderly. <i>Nat. Commun.</i> 13, 6894 (2022). Obermoser, G. et al. Systems Scale Interactive Exploration Reveals Quantitative and Qualitative Differences in Response to Influenza and Pneumococcal Vaccines. <i>Immunity</i> 38, 831–844 (2013).</p>
Data exclusions	No data was excluded from our analysis after quality check.
Replication	<p>All the experiments (functional antibody titer estimation using OPA, flow cytometry, bulk and single cell RNAseq profiling) were performed once in multiple biological replicates, and the analysis showed good correlation between the biological replicates. Flow cytometry assays were performed on fresh blood collected from 39 donors over multiple visits pre-and post-vaccination. Cell staining for</p>

different cell compartments was successfully replicated in multiple donors at the same visit time point throughout the vaccine study.

Randomization Among the recruited older adults, they were randomly assigned to each vaccine arm while trying to balance for biological sex and age and frailty distribution in each arm.

Blinding This is an open label study and not blinded.

Reporting for specific materials, systems and methods

We require information from authors about some types of materials, experimental systems and methods used in many studies. Here, indicate whether each material, system or method listed is relevant to your study. If you are not sure if a list item applies to your research, read the appropriate section before selecting a response.

Materials & experimental systems

Methods

- n/a
- Involvement in the study
- Antibodies
 - Eukaryotic cell lines
 - Palaeontology and archaeology
 - Animals and other organisms
 - Clinical data
 - Dual use research of concern
 - Plants

- n/a
- Involvement in the study
- ChIP-seq
 - Flow cytometry
 - MRI-based neuroimaging

Antibodies

Antibodies used

Marker; Clone; Label; Antibody Registry ID;
 Lin1 (CD3,14,16,19,20,56); CD3(SK7), CD16(3G8), CD19(SJ25C1), CD20(L27),CD14(MΦP9), CD56(NCAM16.2); FITC; BD Biosciences Cat# 340546, RRID:AB_400053;
 CD138; MI15; PerCP-Cy5.5; BD Biosciences Cat# 341097,RRID:AB_400219;
 IgD; IA6-2; FITC; BD Biosciences Cat# 555778, RRID:AB_396113;
 PD-1 (CD279); MIH4; FITC; BD Biosciences Cat# 557860, RRID:AB_2159176;
 CD3; UCHT1; AF700; BD Biosciences Cat# 557943, RRID:AB_396952;
 CCR6 (CD196); 11A9; PE; BD Biosciences Cat# 559562, RRID:AB_397273;
 CD11c; B-ly6; V450; BD Biosciences Cat# 560369, RRID:AB_1645557;
 CD40; 5C3; APC-R700; BD Biosciences Cat# 565179, RRID:AB_2739094;
 CD19; J4-119; ECD; Beckman Coulter Cat# IM2708U, RRID:AB_130854;
 CD45RA; 2H4; ECD; Beckman Coulter Cat# IM2711U, RRID:AB_10640553;
 CD20; 2H7; APC; BioLegend Cat# 302310, RRID:AB_314258;
 ICOS (CD278); C398.4A; PE-Cy7; BioLegend Cat# 313520, RRID:AB_10643411;
 CD4; OKT4; APC-Cy7; BioLegend Cat# 317418, RRID:AB_571947;
 BDCA-1 (CD1c); L161; PerCP-Cy5.5; BioLegend Cat# 331514, RRID:AB_1227535;
 CXCR3 (CD183); G025H7; BV421; BioLegend Cat# 353716, RRID:AB_2561448;
 CD27; M-T271; PE; BioLegend Cat# 356406, RRID:AB_2561825;
 CD86; IT2.2; PE-Cy7; BioLegend Cat# 305422, RRID:AB_2074981;
 CXCR5 (CD185); J252D4; APC; BioLegend Cat# 356908, RRID:AB_2561817;
 BDCA-2 (CD303); AC144 PE; Miltenyi; Biotec Cat# 130-090-511, RRID:AB_244168;
 BDCA-3 (CD141); AD5-14H12; APC; Miltenyi; Biotec Cat# 130-090-907, RRID:AB_244170;
 HLA-DR; LN3; APC-eFluor 780; Thermo Fisher Scientific Cat# 47-9956-42, RRID:AB_1963603;

Validation

All antibodies used were evaluated by the manufacturers as provided in their websites. Refer the link under reference link for the references associated to marker validation.

Marker; Reference

Lin1 (CD3,14,16,19,20,56); <https://wwwbdbiosciences.com/en-us/products/reagents/flow-cytometry-reagents/clinical-discovery-research/multicolor-cocktails-and-kits-ruo-gmp/anti-human-lineage-cocktail-1-lin-1-cd3-cd14-cd16-cd19-cd20-cd56.340546>

CD138; <https://wwwbdbiosciences.com/en-us/products/reagents/flow-cytometry-reagents/clinical-diagnostics/single-color-antibodies-asr-ivd-ce-ivd/cd138-percp-cy-5-5.341097>

IgD; <https://wwwbdbiosciences.com/en-us/products/reagents/flow-cytometry-reagents/research-reagents/single-color-antibodies-ruo/fic-mouse-anti-human-igd.562023>

PD-1 (CD279); <https://wwwbdbiosciences.com/en-us/products/reagents/flow-cytometry-reagents/research-reagents/single-color-antibodies-ruo/fic-mouse-anti-human-cd279.557860>

CD3; <https://wwwbdbiosciences.com/en-us/products/reagents/flow-cytometry-reagents/research-reagents/single-color-antibodies-ruo/alexa-fluor-700-mouse-anti-human-cd3.561027>

CCR6 (CD196); <https://wwwbdbiosciences.com/en-us/products/reagents/flow-cytometry-reagents/research-reagents/single-color->

antibodies-ruo/pe-mouse-anti-human-cd196-ccr6.559562

CD11c; <https://wwwbdbiosciences.com/en-us/products/reagents/flow-cytometry-reagents/research-reagents/single-color-antibodies-ruo/v450-mouse-anti-human-cd11c.560369>CD40; <https://wwwbdbiosciences.com/en-us/products/reagents/flow-cytometry-reagents/research-reagents/single-color-antibodies-ruo/apc-r700-mouse-anti-human-cd40.565179>CD19; <https://elifesciences.org/articles/60939/figures>, <https://www.ncbi.nlm.nih.gov/pmc/articles/PMC7873835/>, <https://pubmed.ncbi.nlm.nih.gov/32661393/>CD45RA; <https://www.ncbi.nlm.nih.gov/pmc/articles/PMC6076291/>, <https://www.nature.com/articles/s41467-022-32491-x>, <https://www.nature.com/articles/s41467-022-32491-x>CD20; <https://www.biolegend.com/en-us/products/apc-anti-human-cd20-antibody-557>CD38; <https://www.biolegend.com/en-us/products/brilliant-violet-421-anti-human-cd38-antibody-7145>ICOS (CD278); <https://www.biolegend.com/en-us/products/pe-cyanine7-anti-human-mouse-rat-cd278-icos-antibody-6908>CD4; <https://www.biolegend.com/en-us/products/apc-cyanine7-anti-human-cd4-antibody-3658>BDCA-1 (CD1c); <https://www.biolegend.com/en-us/products/percp-cyanine5-5-anti-human-cd1c-antibody-5182>CXCR3 (CD183); <https://www.biolegend.com/en-us/products/brilliant-violet-421-anti-human-cd183-cxcr3-antibody-7712>CD27; <https://www.biolegend.com/en-us/products/pe-anti-human-cd27-antibody-8371>CD86; <https://www.biolegend.com/en-us/products/pe-cyanine7-anti-human-cd86-antibody-3961>CXCR5 (CD185); <https://www.biolegend.com/en-us/products/apc-anti-human-cd185-cxcr5-antibody-8360>BDCA-2 (CD303); <https://www.miltenyibiotec.com/US-en/products/cd303-bdca-2-antibody-anti-human-ac144.html#conjugate=pe:size=100-tests-in-200-ul>BDCA-3 (CD141); <https://www.miltenyibiotec.com/US-en/products/cd141-bdca-3-antibody-anti-human-ad5-14h12.html#conjugate=apc:size=100-tests-in-200-ul>HLA-DR; <https://www.thermofisher.com/antibody/product/HLA-DR-Antibody-clone-LN3-Monoclonal/47-9956-42>

Clinical data

Policy information about [clinical studies](#)

All manuscripts should comply with the ICMJE [guidelines for publication of clinical research](#) and a completed [CONSORT checklist](#) must be included with all submissions.

Clinical trial registration

Study protocol

Data collection

Outcomes

Flow Cytometry

Plots

Confirm that:

- The axis labels state the marker and fluorochrome used (e.g. CD4-FITC).
- The axis scales are clearly visible. Include numbers along axes only for bottom left plot of group (a 'group' is an analysis of identical markers).
- All plots are contour plots with outliers or pseudocolor plots.
- A numerical value for number of cells or percentage (with statistics) is provided.

Methodology

Sample preparation

Fluorescent-labeled antibody cocktails for different cell-surface staining panels were pre-mixed in BD Horizon Brilliant Stain Buffer (BD Biosciences) 10 minutes before staining. Antibody cocktails were added over 100 μ L aliquots of anticoagulated whole blood in a 5 ml FACS tube within 60 minutes of blood collection. Samples were incubated for 15 minutes at room temperature then lysed and fixed with 2 ml of 1x FACS lysing solution (BD Biosciences) for 8 minutes at room temperature. The lysed samples were washed twice to remove the unbound antibodies, lysed RBCs, and platelets and finally resuspended in 250 μ L of PBS to which 50 μ L of count beads suspension (Count Bright Absolute Counting Beads, Thermo Fisher) were added for the detection of absolute cell counts.

Instrument

BD LSR Fortessa X-20

Software

Data were acquired using BD FACS Diva and the analyzed using FlowJo V9.9.6 software.

Cell population abundance

No cell sorting procedure was used in the study.

Gating strategy

1. CD4+ T cell compartment
 - a. Bulk blood cells via FSC-A vs SSC-A.
 - b. Doublets exclusion via FSC-H vs FSC-A.
 - c. CD4 gating via CD3 vs CD4 of the gated Singlets
 - d. Memory CD4 via CD4 vs CD45RA of the gated CD4
 - e. Th and Tfh via CD4 vs CXCR5 of the gated Memory CD4
 - f. Th1/Th2/Th17/Th1-Th17 via CXCR3 vs CCR6 of the gated Th
 - g. Tfh1/Tfh2/Tfh17/Tfh1-Tfh17 via CXCR3 vs CCR6 of the gated Tfh
2. B cell compartment
 - a. Bulk blood cells via FSC-A vs SSC-A.
 - b. Doublets exclusion via FSC-H vs FSC-A.
 - c. CD19 gating via CD3 vs CD19 of the gated Singlets
 - d. Memory CD19 via IgD vs CD27 of the gated CD19
 - e. CD20(-) Memory CD19 via CD19 vs CD20 of the gated Memory CD19
 - f. Plasmablast/Plasmacell via CD38 vs CD138 of the gated CD20(-) Memory B cells
3. DC compartment
 - a. Bulk blood cells via FSC-A vs SSC-A.
 - b. Doublets exclusion via FSC-H vs FSC-A.
 - c. HLA-DR(+)Lineage(-) via HLA-DR vs Lin of the gated Singlets
 - d. CD11c(+) and BDCA2(+) via CD11c vs CD303 of the gated HLA-DR(+)Lineage(-)
 - e. cDC1 and cDC2 via CD1c vs CD141 of the gated Memory CD11c(+).

- Tick this box to confirm that a figure exemplifying the gating strategy is provided in the Supplementary Information.